Hindawi Publishing Corporation
International Journal of Optics
Volume 2011, Article ID 293684, 20 pages
doi:10.1155/2011/293684

Review Article

Biophotonics Modalities for High-Resolution Imaging of Microcirculatory Tissue Beds Using Endogenous Contrast: A Review on Present Scenario and Prospects

Hrebesh M. Subhash

Biophotonics and Functional Imaging Laboratory, Division of Biomedical Engineering, School of Medicine, Oregon Health and Science University, 3303 SW Bond Avenue, Portland, OR 97239, USA

Correspondence should be addressed to Hrebesh M. Subhash, hrebeshms@gmail.com

Received 20 October 2010; Revised 23 February 2011; Accepted 10 March 2011

Academic Editor: Armando Nolasco Pinto

The microcirculation is a complex system, and the visualization of microcirculation has great significance in improving our understanding of pathophysiological processes in various disease conditions, in both clinical and fundamental studies. A range of techniques are available or emerging for investigating different aspect of the microcirculation in animals and humans. This paper reviews the recent developments in the field of high-resolution and high-sensitive optical imaging of microcirculatory tissue beds, emphasizing technologies that utilize the endogenous contrast mechanism. Optical imaging techniques such as intravital microscopy, Capillaroscopy, laser Doppler perfusion imaging, laser speckle perfusion imaging, polarization spectroscopy, photoacoustic tomography, and various implementations of optical coherence tomography based on Doppler and speckle contrast imaging are presented together with their prospectives and challenges.

1. Introduction

The microcirculation plays a vital role in the pathophysiology of several disorders in many clinical areas including cardiology, dermatology neurology and ophthalmology, and so forth. [1]. The primary function of microcirculation is referred to the process involved in the nutritive blood delivery to the tissue's capillary bed, which is vital for the homeostasis, and thereby the survival of an organ. Recent advances have highlighted the crucial involvement of the microcirculation in many basic research and clinical circumstances including cancer diagnosis and therapy, arteriosclerosis, therapeutic angiogenesis, vasopastic conditions, reconstructive surgery, and also for development and implementation of anti-vascular strategies. In clinical research, noninvasive imaging of microcirculation could be of great significance in accessing the effect of medical or surgical intervention in clinical trials, and in clinical practice it could be helpful to assist in diagnosis and monitoring of disease progression or the result of therapy in individual patients. Numerous imaging techniques have been proposed in the last few decades to image microcirculation in medical research area, which vary widely by the type of microcirculatory information that they can provide and in their cost and availability.These methods includes positron emission tomography (PET) [2], Magnetic resonance imaging (MRI) [3], plethysmography [4, 5], thermal [6] and radioisotope [7, 8] clearance, orthogonal polarization spectral imaging [9, 10], video-photometric capillaroscopy [11, 12], and Doppler ultrasound [13]. Some of these methods are limited with their imaging parameters such as spatial and temporal resolution, quantification of flow information, capability of obtaining depth resolved information, chronic imaging of tissue perfusion, injection of labeled pharmaceuticals for enhanced contrast, and the level of noninvasiveness; others have practical limitations in clinical and basic research applications. There has been a great deal of interest in developing non/minimally-invasive high-resolution label-free depth-resolved imaging modality for clinical and fundamental studies.

In general, imaging microcirculation is a very challenging task due to the requirement of relatively high spatiotemporal resolution and sensitivity to image small diameter of the blood vessels. Most of the available methods that fulfill these conditions are based on optical measurement technologies. The currently existing high-resolution optical imaging techniques can be broadly classified into two categories; the first one generally require invasive procedures or exogenous contrast agents, such as fluorescence angiography, intravital confocal microscopy and two-photon excitation microscopy, and so forth, which perturb the intrinsic physiology of the microcirculation. The second one is based on endogenous contrast and direct visualization of microcirculation such as laser Doppler technique, infrared thermography, Nail fold video microscopy, capillaroscopy, polarization spectroscopy, optical intrinsic signal imaging, photo acoustic imaging and phase-resolved Doppler optical coherence tomography, and so forth. [15–19]. In this paper we will provide an overview of various types of optical imaging modalities that are based on endogenous contrast mechanism for imaging of microcirculation. The review will also focus on the recent technical advances in the field of OCT-based flow imaging modalities and will highlight various Doppler and speckle contrast-based OCT imaging techniques which have most significant impact in the present scenario of endogenous-based microcirculation imaging.

2. Conventional Endogenous Contrast Based Optical Imaging Optical Imaging Modalities for Microcirculation Imaging

2.1. Video Capillaroscopy. Video capillaroscopy [20, 21] is a widely used noninvasive high-resolution optical microscopic imaging modality in clinical routine and dermatology research. Video capillaroscopy may also be referred to as intravital capillary microscopy or intravital capillaroscopy although in the clinical setting "intravital" is often omitted. Video capillaroscopy allows visualization of a living system in real-time, especially the nutritional dermal capillaries, which is clinically important in several pathological circumstances like skin lesion, pressure ulcers, or diabetes [22, 23]. Video capillaroscopy provides a two-dimensional projection map of a three-dimensional network of capillaries. In combination with television and video and/or computer technology, a typical video capillaroscopy setup provides high contrast images of skin capillaries on videotape, computer disc, or photograph. Fiber optics illumination is commonly used to illuminate the imaging sample. In clinical diagnostics, capillaroscopy is widely used in certain specific places in the body such as the area of skin overlapping the base of the finger nail and toe nail, pigmented skin lesion area where capillaries come close enough to the surface of the skin. During imaging to increase the transparency of the tissue, a clearing agent such as index matching oil or immersion oil is often used [24, 25]. The video capillaroscopy may be used to assess different parameters such as capillary morphology, capillary density, and capillary red cell column width. However, in certain types of highly pigmented skin, the pigment, melanin absorbs light very strongly in the visible spectrum making capillaroscopy difficult. In such condition, the capillaroscopy in conjunction with intravenous administration of fluorescence dyes (sodium fluorescein or indocynide green), this is one of the main limitation of capillaroscopy. Furthermore, sodium fluorescein dye may cause nausea, vomiting, itching, dyspnea, and additional adverse allergic reactions [26], while indocyanine green dye must be used cautiously in patients who are allergic to iodine and shellfish [27]. Another main disadvantage is that this method cannot provide depth information. The nail fold microcirculation is extremely sensitive to external temperature and vasoconstrictive agents [28]. It has also been reported that nail fold microvascular blood flow was reduced in normotensive febrile patients [29]. The use of this technique in man is limited to the easy accessible surfaces such as the skin, nailfold, lip, or the bulbar conjunctiva [30, 31]. Thus, the nailfold videomicroscopy may not be a reliable indicator of microcirculation in other parts of the body, particularly in critically ill patients. Figure 1 shows the videocapillaroscopy image of nailfold region of a normal human volunteer.

2.2. Intravital Confocal Microscopy (IVM). The gold standard for assessment of microcirculation is intravital confocal microscopy [33, 34], which has been widely used in small animal studies to examine the microcirculations *in situ* and *in vivo* with high resolution. The technique is feasible with inherently thin tissues which allow transillumination, such as tadpole tail and bat wing. Intravital microscopy can provide quantification of vessel count, diameter, length, density, permeability, and blood flow velocity. However, intravital microscopy is a time consuming, invasive procedure, and the imaging depth is limited to a few hundred microns in highly scattering specimens [35]. The intravital microscopic study of the microcirculation without the use of dyes in humans has been largely restricted to the very superficial layers. Moreover, the size and flexibility of instrument for clinical and research studies can also be a limiting factor.

2.3. Orthogonal Polarization Imaging (OPS). Orthogonal polarization spectral (OPS) imaging is a relatively new technique, which allows direct visualization of the microcirculation without using any florescent dye [36, 37]. Unlike conventional reflectance imaging (CRI), OPS uses the phenomenon of cross-polarization to reduce the multiple surface scattering and turbidity of the surrounding tissues. In OPS imaging linearly polarized light is used to image the sample, and most of the light that reflects back from the superficial layers retain the same polarization of the imaging beam; however, the light that penetrates the tissue more deeply undergoes multiple scattering events and becomes depolarized. Using sophisticated orthogonal polarization optics only the depolarized scatted light which is emerging from the deeper tissue layers is extracted and imaged on to a two-dimensional array detector. In general, wavelengths at isosbestic point of hemoglobin absorption were chosen to achieve optimal imaging of the microcirculation because

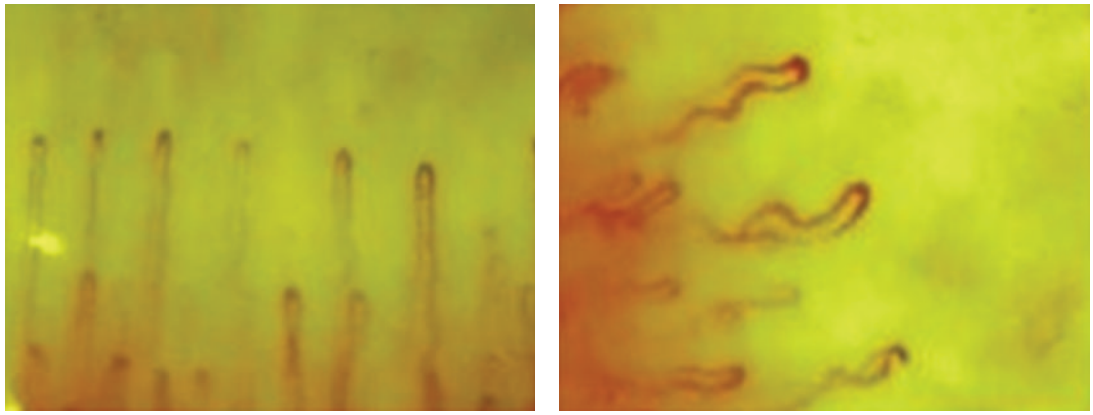

(a) (b)

Figure 1: Videocapillaroscopy image of nail fold region of a normal human volunteer (magnification × 200). The image clearly reveals the morphological microvascular patterns in the nail fold.

at this wavelength oxy- and deoxy-hemoglobin absorb the light equally. Thus, the blood vessels of the microcirculation can be visualized by OPS imaging. However, OPS provide no depth resolved information and lacks the measurement consistency [38] required for longitudinal studies.

2.4. Laser Doppler Imaging (LDI). Convectional laser Doppler flowmetry [39–41] is used to monitor the microvascular function by measuring the red cell flux in small volume samples of tissue surface. This method operates on the basis of frequency shift produced by the Doppler Effect to image the microvascular. The flow map corresponds to a quantity referred as perfusion, which is defined as the product of local speed and concentration of blood cells, and recoded the integrated perfusion within a sample volume. Unlike conventional laser Doppler perfusion monitoring, which uses a single pot measurements of perfusion changes in tissue, LDI uses a sequential scan on the tissue surface to provide a color coded, two-dimensional image of tissue perfusion without disturbing the tissue of interest. There are different scanning modalities have been developed for producing two-dimensional perfusion map, such as point-raster scan technique, line-scanning technique, and full-field scanning technique [42–46]. This technique is capable of noninvasive and continuous recording of blood perfusion in many clinical applications. However, LDI is still not has been fully integrated into clinical setting and is mainly used fundamental and research studies. A major limitation of LDI is its inability to provide depth resolved perfusion map and imaging depth is limited to only around 1 mm [39]. Moreover, Laser Doppler is not able to measure flow in absolute unit (i.e, mL/min), thus it often uses arbitrary unit of flux, which is the product of concentration of moving blood cells and the mean velocity of those blood cells [39].

2.5. Laser Speckle Perfusion Imaging (LSPI). Laser speckle perfusion imaging is another alterative laser-based microcirculation imaging modality [47, 48], which uses the decorrelation of the speckle pattern over the finite integration of the two-dimensional detector array to quantify the blood flow. Based on the local contrast calculation, various implementations of LSI methods are reported in the literature. One of the most widely used LIS method is Laser Speckle Contrast Analysis (LASCA), in this modality the local contrast is computed in a block of $n \times n$ pixels from digital speckle photograph [49–51]. Due to the fact that the contrast in LASCA is analyzed for a group of pixels in one image, this modality has the disadvantage of a lack of spatial resolution. In order to overcome this limitation, another modality called Laser Speckle Imaging (LSI) has been proposed [52–54]. In LSI imaging modality, the local contrast is calculated based on one pixel in a time sequence, rather than based on multiple pixels in one image in LASCA. However, the main limitation of LSPI is that it can produce good measures of relative two-dimensional projection map of flow and cannot provide the baseline flow information. This is because it is still unknown which velocity distribution (e.g., Voigt, Lorentzian, or Gaussian) should be used. Thus, LSPI method needs to assume a specific velocity distribution to relate the speckle contrast to the tissue perfusion, and this makes the technique less generally applicable. Another major limitation of LSPI is k of knowledge of the depth resolved flow information and the biological zero signal, which arises from the perfusion measured at no flow condition. Figure 2 shows the LSI image of mouse brain perfusion with intact skull (The image is from unpublished work by the author).

2.6. Photo Acoustic Tomography (PAT). Photoacoustic tomography (PAT) [55, 56], based on thermal-acoustic phenomena resulting from the strong light absorption of blood and the subsequent thermoelastic expansion, which has been reported to map vascular structures deep within the brain of small animals [57]. There are basically two types of PA imaging techniques: PA microscopy (PAM) and PA Tomography. PAM uses spherically focused ultrasonic transducers with 2D point-by-point scanning to localize the PA sources

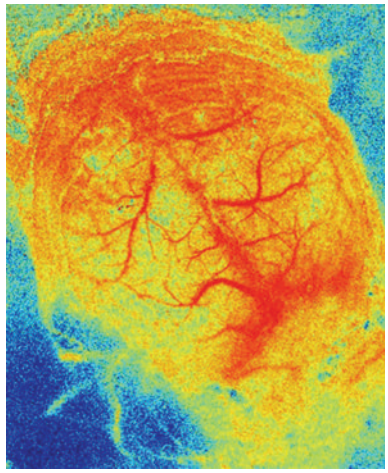

Figure 2: Laser speckle imaging (LSI) of blood flow dynamics in the mouse brain through intact skull ($10 \times 8.5\,\text{mm}^2$).

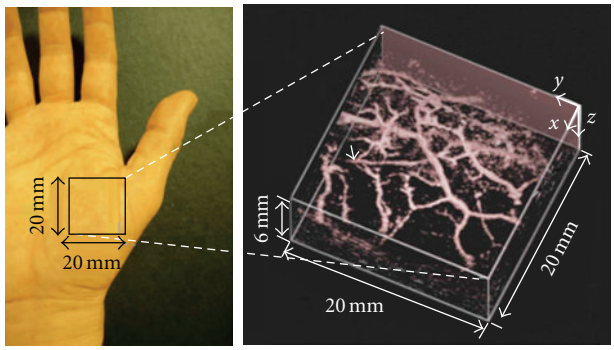

(a) (b)

Figure 3: Fabry-Pérot interferometer-based PAT of the vasculature in a human palm *in vivo*. Excitation wavelength is 670 nm. (a) Photograph of the imaged region (b). Volume rendered image. Reproduced with permission from [14].

in linear or sector scans and then reconstruct the 3D high-resolution tomographic image directly from the measured data set [58]. Recently, optical resolution PAM cable of imaging single capillaries *in vivo* with a resolution of ~5 μm was reported [59]. On the other hand, PAT uses pulsed broad laser beam, which illuminates the biological tissue under investigation to generate a small but rapid temperature rise, which leads to emission of ultrasonic waves due to thermoelastic expansion [60, 61]. A typical PAT system uses an unfocused (wideband) ultrasound detector to detect the short-wavelength pulsed ultrasonic waves. High-resolution tomographic images of optical contrast are then formed through image reconstruction. This endogenous optical contrast of PA signal can be used to quantify the concentration of total hemoglobin, the oxygen saturation of hemoglobin, and the concentration of melanin. However, because of the use of ultrasound, PAM and PAT inherit the requirement of an acoustic coupling medium for imaging, which is one of the major limitation that are associated with the ultrasound technology. In addition, the spatial (~100 μm) resolution limit of PAT is limited by the viscoelastic filtering of higher acoustic frequencies by the tissue. Moreover, quantification of flow velocity based on Doppler imaging has yet to be explored beyond the realm of PA imaging. Figure 3 shows the volume rendered PAT image of the vasculature in a human palm *in vivo*.

3. Mcrocircualtion Imaging Based on Optical Coherence Tomography (OCT)

Optical coherence tomography (OCT) is a novel, noninvasive, optical imaging modality based on low coherence interferometry [18, 62–64]. The principle of OCT was first conceived in 1990 by Dr. Naohiro Tanno, a professor at Yamagata University [65, 66], and then perfected in 1991 by Massachusetts Institute of Technology team headed by Professor James Fujimoto [62]. OCT enables the noninvasive, noncontact imaging of cross-sectional structures in biological tissues and materials with high resolution. In principle, OCT is an optical analogue to clinical ultrasound. In OCT, the temporally gated optical pulse remitted from scattering sites within the sample is localized by low-coherence interferometry (LCI) [67–75]. This is typically achieved with a Michelson interferometer. The sample rests in one arm of the interferometer, and a scanning reference optical delay line is in the other arm. In LCI, light interferes at the detector only when light reflected from the sample is matched in optical pathlength with that reflected from the scanning reference mirror. A single scan of the reference mirror thus provides a one-dimensional depth-reflectivity profile of the sample. Two-dimensional cross-sectional images are formed by laterally scanning the incident probe beam across the sample. The reconstructed OCT image is essentially a map of the changes of reflectivity that occurs at internal interfaces, similar to the discontinuities in acoustic impedance in ultrasound images.

A typical implementation of OCT imaging system comprises a broadband light source emitting light of high spatial and low temporal coherence, which is coupled into a 2×2 fiber optics-based Michelson interferometer, as shown in Figure 4. The Michelson interferometer divides the light beam and directs it into two arms of the interferometer. The sample arm beam directs into the object to be analyzed. It usually contains collimating optics enabling formation of a narrow beam, which penetrates the object. In order to reconstruct two-dimensional cross-sectional images of the object, the beam is galvanometrically scanned across the sample surface. Light backscattered or reflected from the various structures returns to the interferometer and is brought to interference with light reflected back from the reference arm mirror (RM. The standard fiber-optics Michelson interferometer is not the most efficient design for practical implementation, because a major disadvantage of this configuration is that the dc signal and intensity noise generated by the light from the reference arm add to the interference signal. In OCT, the coherence-gated information about the elementary volume of the scatters within the obscuring scattering specimen can be obtained

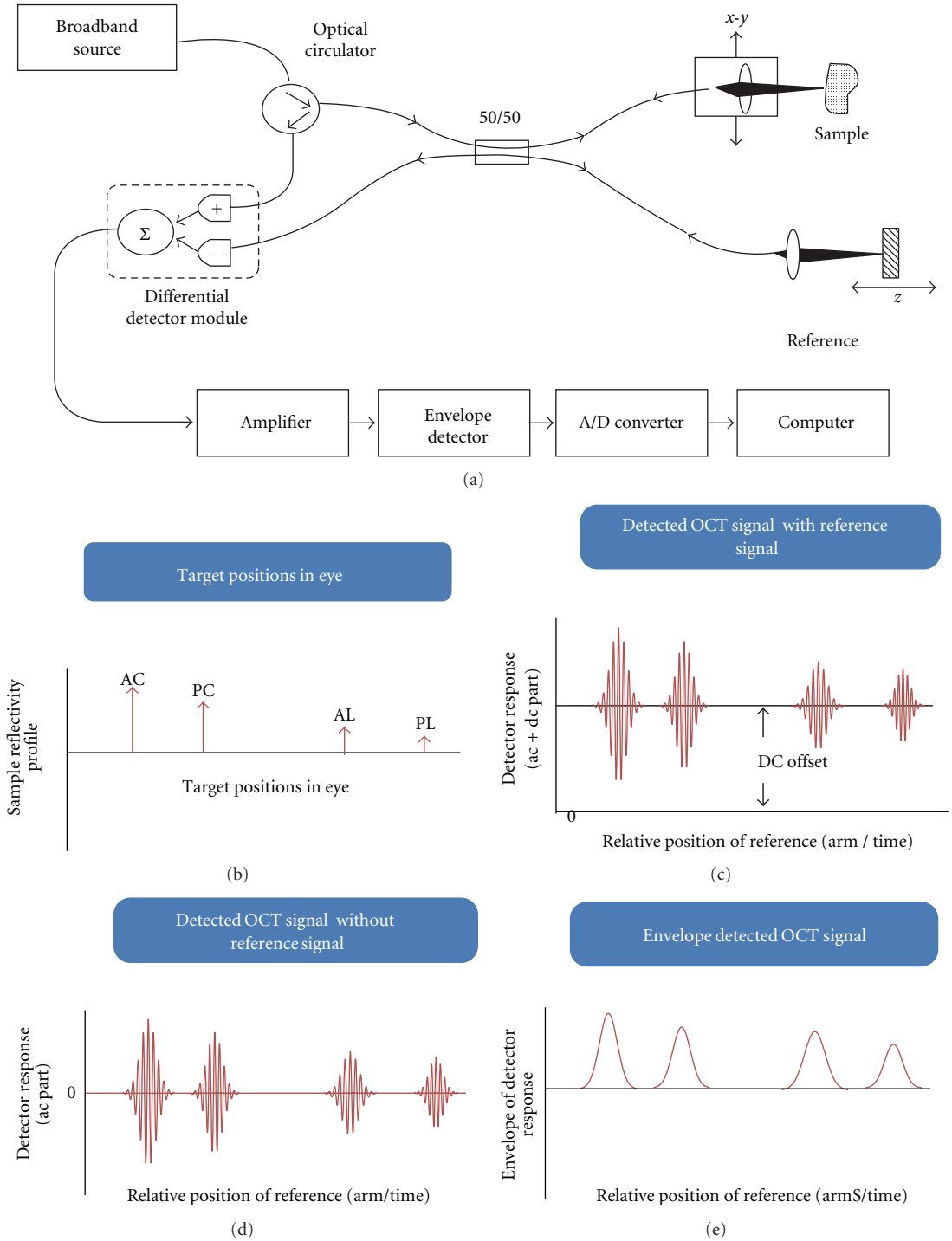

Figure 4: (a) Schematic of a typical fiber optics-based time-domain OCT setup. (b) Reflectivity profile of target position in the ocular medium. (c) Detected interference signal by the photodetector. (d) Detected signal with reference signal filtered out. (e) Demodulated and envelop detected OCT signal.

from either the time domain measurement (TD-OCT) or the frequency domain (FD-OCT) [76, 77] measurement. As a variant coherence domain variant interferometric imaging modality, FD-OCT has been widely attracted in the biomedical imaging field due to its higher sensitivity and imaging speed compared to conventional TD-OCT. The principle of FD-OCT relies on the transformation of the OCT time varying signal along the optical axis, termed the A-scan, into the frequency domain.

In contrast to standard microscopy, OCT can achieve fine axial resolution independent of the beam focusing and spot size. The axial image resolution in OCT is determined by the

measurement resolution for echo time delays of light. The axial resolution of an OCT is an important specification of an OCT system, and in many biomedical applications high axial resolution is often required to distinguish different cellular ultrastructures. The axial resolution of OCT is defined as the full width half maximum (FWHM) of the source coherence length l_c. For a source with a Gaussian spectral distribution, the axial resolution is given by

$$\Delta z = \frac{2\ln 2}{\pi}\frac{c}{\Delta \nu} = \frac{2\ln 2}{\pi}\frac{\lambda^2}{\Delta\lambda} \approx 0.44\frac{\lambda^2}{\Delta\lambda}. \quad (1)$$

where Δz and $\Delta\lambda$ are the full width at half maximum of the autocorrelation function and spectral width and λ_0 is the source center wavelength [66]. It can be seen that broadband light sources are required to achieve high axial resolution, as the axial resolution is inversely proportional to the spectral width of the light source. The transverse resolution in OCT imaging is the same as in optical microscopy and is determined by the diffraction limited spot size of the focused optical beam. The diffraction limited minimum spot size is inversely proportional to the numerical aperture or the focusing angle of the beam. The lateral resolution Δx can be written as

$$\Delta x = \frac{4\lambda}{\pi}\left(\frac{f}{d}\right), \quad (2)$$

where f is the focal length of the objective lens and d is the $1/e^2$ Gaussian beam wrist at the objective lens. It can be seen from the above equation that high lateral resolution can be achieved by using a large numerical aperture (NA) to decrease the spot size. However, for the selection of optics there is a trade-off between the lateral resolution and the imaging depth. A higher lateral resolution leads to a decrease in the depth of focus, or confocal parameter b, which is twice the Rayleigh range

$$2\Delta z_R = b = \frac{\pi\Delta x^2}{2\lambda}. \quad (3)$$

The Rayleigh range gives the distance from the focal point to the point where the light beam diameter has increased by a factor of $\sqrt{2}$. This effectively limits the scanning range of the OCT, quite apart from the working range of the scanning reference delay line, as it is the range over which lateral resolution is maintained.

Soon after the invention of OCT, there has been a great interest in the development of various hardware and software modules for extending the functionality of OCT for measuring functional and physical parameters such as such as polarization sensitive [78–89], Doppler flow imaging [90–95], spectroscopy [96–101], elastography, and so forth. Among them microvascular imaging of flow based on OCT is a major trust area of research. The microvascular imaging modality based on OCT can be broadly divided into two categories, the one based on Doppler principle, that generally quantifies the blood flow velocity, and the one based on speckle contrast imaging principle, which is mainly used for the visualization of microvascular blood circulation without providing any quantitative flow information. A number of extensions of flow imaging modalities based on OCT have been implemented using the above mentioned principles. In the following section we will provide an over view of some of the prominent techniques.

3.1. Doppler OCT (D-OCT). Doppler optical coherence tomography (DOCT) is an alternative low coherence interferometric technique to extract depth-resolved blood flow information in functional vessels within the tissue beds. Recently, DOCT have received extensive attention over other label-free optical imaging techniques and found numerous applications in various fundamental biology and clinical studies because of many advantages, such as high spatial and temporal resolution, noncontact, noninvasiveness, depth resolvability, flexibility with integrating with clinical surgical systems, and the capability to providing real-time measurement with high speed and sensitivity. The operating principle of DOCT is fundamentally very similar to the Doppler velocimetry. Doppler velocimetry suffers from imprecise imaging due to the long coherence length of the light source used, which results the interference of the static and Doppler shifted components of light occurs over a long optical path. However, in DOCT the low coherence gating property of OCT overcomes this problem, thus permitting quantitative imaging of fluid flow in highly scattering media, such as monitoring *in vivo* blood flow beneath the skin.

In DOCT, the velocity resolution depends upon detection electronics, scan angle, and acquisition time. Reported flow velocity resolutions are in the region 10–100 μms^{-1}; based on first generation time-domain OCT systems [90–92]. However, recent development in Fourier Domain Doppler OCT (FD-DOCT) has shown that a velocity resolution of just a few micrometers per second may be achieved [32, 102–105]. The DOCT can provide 3D-tomographic map and velocity profile of blood flow in tissue, which attracted a number of biomedical applications, for example, determination of the depth of burns, determining tissue perfusion to ensure adequate oxygenation of the tissue after injury, wound closure, grafting, and so forth. Other applications include distinguishing between arterial and venous blockages in tissue after injury, or monitoring the effect of pharmaceuticals on blood transport in the tissues. A typical cross-sectional DOCT image of the flow characteristics in a standard circular plastic tube is shown in Figure 5(a). Figure 5(b) shows the 3D flow velocity plot for the area marked by the dashed box in Figure 5(a), and the inset in Figure 5(b) shows the velocity plot across the channel of the tube indicated by the dashed line.

3.1.1. Doppler OCT Principle. The basic principle behind DOCT is Doppler effect, which describes the shift in frequency of waves reflected from moving objects. This frequency shift can be used to determine object-moving velocity. For electromagnetic waves such as light, derivation of the Doppler shifted frequency from a moving object

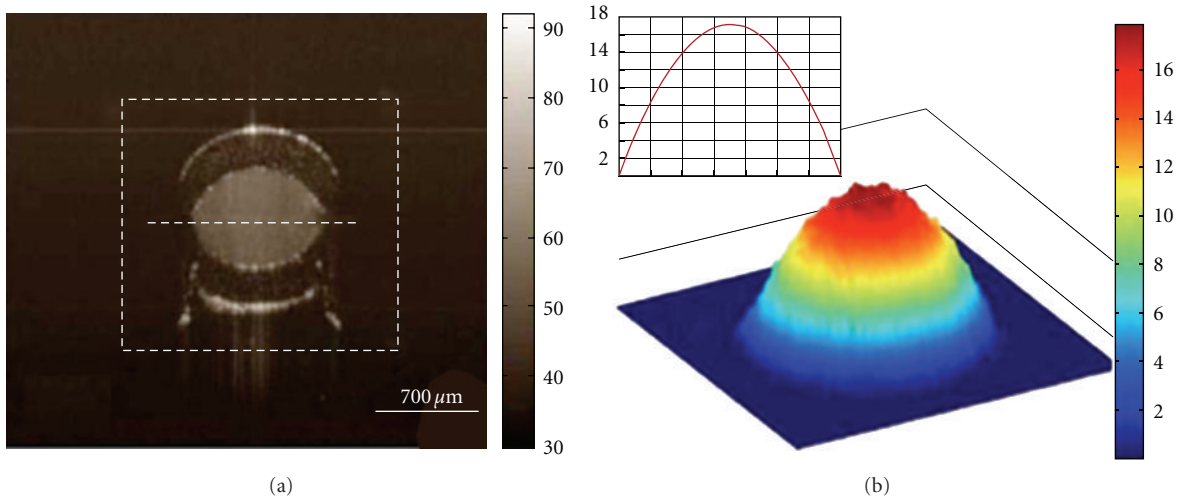

(a) (b)

Figure 5: (a) 2D cross-sectional DOCT image of the flow characteristics in a standard circular plastic tube. (b) 3 D flow velocity plot for the area marked by the dashed box in (a). The inset in (b) shows the velocity plot across the channel of the tube indicated by the dashed line in (a).

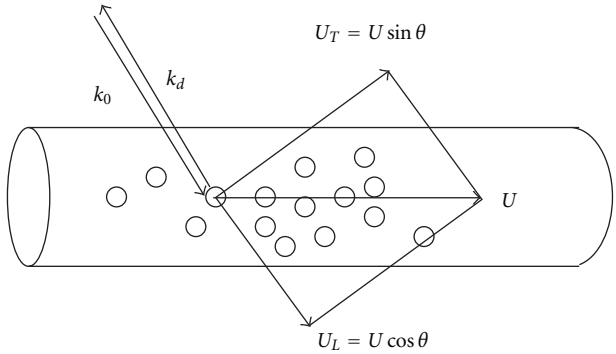

Figure 6: Schematic for optical Doppler tomography. The sample arm beam is held at some angle θ to the direction of flow. Therefore, an optical signal with wave-vector k_0 falls on a particle moving with velocity u. The light scattered back into the sample objective is Doppler shifted and has wave-vector k_d.

requires the application of special relativity. The result for a Doppler shifted frequency f_d is

$$f_d = \sqrt{\frac{c+u}{c-u}} f_0, \tag{4}$$

where f_0 is the initial frequency of the electromagnetic wave, c the speed of light, and u is the speed of the moving object. Here, it is assumed that u is positive when the object is moving towards the observer. In this case, it is seen that the Doppler shifted frequency, Δf, must be greater than the initial frequency

$$\Delta f = f_d - f_0. \tag{5}$$

It can be shown that when u is much less than c, the velocity of the moving sample is given by

$$\Delta f = \frac{u}{c} f_d. \tag{6}$$

In the practical DOCT system, Figure 6, the interferometer sample arm is angled relative to the direction of flow by an amount θ. Detected light is scattered from a moving particle in the sample, undergoing a double Doppler shift—once from the source to the particle, and once again from the particle back to the objective. These two factors are taken into account by expressing (6) in terms of initial source and scattered wave-vectors k_0 and k_d, respectively. The Doppler shift can then be written as

$$\Delta f = \frac{1}{2\pi}(k_d - k_0) \cdot u. \tag{7}$$

Therefore, the velocity of moving particles can be determined from the measurement of the Doppler shift and knowledge of the relative angle between the optical signal and the flow [44]

$$u = \lambda_0 \frac{\Delta f}{2\cos(\theta)}. \tag{8}$$

Using OCT structural information about the sample is obtained by either conventional TD-OCT [62] or more recently FD-OCT [76]. However, to retrieve data regarding the flow of particles within submerged capillary, extra measurements of the Doppler shifted frequency must be made. To do this in the time domain, the reference mirror of the interferometer is scanned to match the path length within the capillary. At each spatial point within the capillary, the detector intensity is sampled at a rate not less than two samples per time period of the source. The time varying result is then Fourier transformed to give the Doppler frequency shift due to moving particles within the capillary. By doing this at a number of points within the capillary, a profile of particle flow is determined.

The axial resolution of DOCT is again dependent on the source temporal coherence length, and the lateral scan resolution on the beam spot size. Velocity resolution depends upon the detection electronics, scan angle, and the

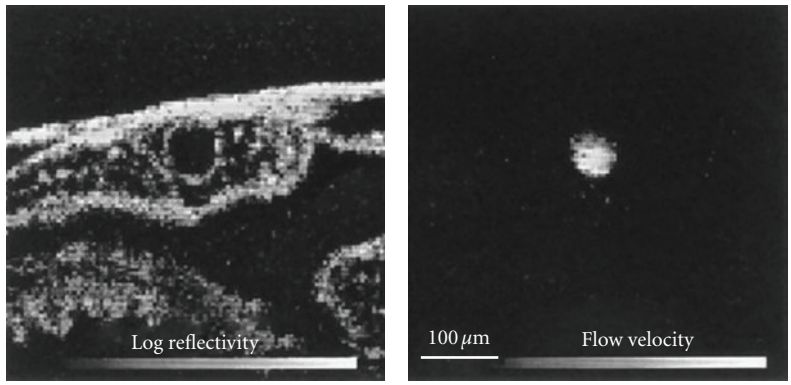

(a) (b)

Figure 7: ODT structural (a) and velocity (b) images of aortic blood flow in Xenopus leaves. Reproduced from [32] with permission.

acquisition time. Reported flow velocity resolutions are in the region 10–100 μms^{-1}; however, recent developments in Fourier domain DOCT (FD-DOCT) have shown a velocity resolution of just a few micrometers per second. FD-DOCT has also shown greater sensitivity in the region of 90–115 dB. The D-OCT image color-codes Doppler shift and, hence, flow velocity. The flow generated was at Reynolds number 2000 and, hence, shows a parabolic flow profile. DOCT has been applied to a number of medical situations, especially in the field of clinical ophthalmology. Not least of these, imaging *in vivo* blood flow in the mouse brain [32], skin [106], and retina [103] has been demonstrated. The capability of DOCT to measure flow within a scattering sample also has potential in new areas of research such as microfluidics [107]. In the following section, we will provide a detailed description about DOCT principle and various flow imaging modalities based on DOCT in both time and frequency domain.

3.1.2. Doppler-Based OCT Flow Imaging Modalities. Soon after the invention of laser in 1960, there has been several attempts to develop Doppler-based optical flow measurement techniques such as laser Doppler velocimeter (LDV), laser speckle contrast imaging, Laser Doppler flowmetry, and so forth. However, the main concern among these methods is the capability of depth resolvability. The localized velocity measurement based on low coherence interferometry was first reported by Gusmeroli and Martinelli in 1991 [108]. The introduction of OCT in to the depth resolved flow imaging techniques represents a major methodological enhancement and a wide verity of novel and advanced DOCT modalities are presently under development. We will provide a short overview of some of the most significant and promising flow imaging modalities based on DOCT.

(1) Time Domain DOCT Modalities

(a) *Spectrogram (Centroid) Method.* The original development of DOCT was based on spectrogram (Centroid). The spectrogram method measurement of the Doppler shifted spectrum at each positions along A-scan (axial the depth) positions provides the velocity profile. A spectrogram [109] is an estimation of the power spectrum of the interference fringe intensity in successive time segments (t_i, $t_i + \Delta t_p$), which can be represented by a two-dimensional surface in the time-frequency plane containing the time-varying spectral properties of the Doppler signal current. Chen et al. first demonstrated the spectrogram method to measure the one-dimensional depth profile of fluid flow velocity in a transparent glass and turbid collagen conduits using DOCT [90]. To construct a spectrogram, the Fourier transform is applied to "short-time" (i.e., localized or windowed) segments of the Doppler signal current. Each local Fourier transform provides the spectral information for that particular time segment, and the window is then shifted to a slightly later time to generate another local spectrum. Following this approach, the properties of the signal can be simultaneously analyzed in the temporal and frequency domains. Although a number of algorithmic approaches can be used to estimate the spectrogram of a time varying signal, short time fast Fourier transform (STFFT) analyses on the time domain interferogram signals [90, 92] were initially adopted in DOCT. Chen et al. first introduced the two-dimensional *in vivo* Doppler OCT imaging using the spectrogram method [110] in 1997. The spectrogram method uses a short time fast Fourier transformation (STFFT) or wavelet transformation to determine the power spectrum of the measured fringe signal. Figure 7(a) shows the structural morphologies of the aorta, and Figure 7(b) shows the high-contrast imaging of aortic blood flow velocity using the spectrogram method.

Izatt et al. demonstrated the feasibility of STFT with complex demodulated A-scans to provide directional flow information in biological tissues with microscale resolution [92]. The complex envelope of the detected interferogram was obtained with a phase-sensitive demodulation technique. The authors showed the color coded 2D Doppler velocity data of a hamster skin-flap model with the color coding indicates direction of flow. Although spectrogram methods allow simultaneous imaging of *in vivo* tissue structure and flow velocity, however, it was quickly realized that STFFT method has severe limitation on real-time *in vivo* imaging of blood flow, largely due to the coupling issue

between the flow imaging resolution and the short time Fourier window size that can be used for flow analyses [32].

(b) *Phase-Resolved DOCT (PRDOCT).* As mentioned above, one of the main drawbacks of STFT-based DOCT is that the velocity sensitivity and spatial resolutions are coupled, that is, a large pixel-time window size increases the system velocity sensitivity while decreasing spatial resolution, meanwhile increasing the image frame rate also decrease the velocity sensitivity. Thus for measuring the blood flow in small vessels in which red blood cells are moving at very low velocity, the imaging frame rate should be reduced. In real-time implementation of DOCT with STFT-based spectrogram method the time for each A-scan is very shot because of the fast frame rate; thus, the velocity sensitivity decreases drastically because the window time for each pixel should be too short to provide the Doppler shift by STFT algorithm. To overcome this limitations, Zhao et al. proposed the phase-resolved DOCT (PRDOCT) method [111], in which by evaluating the phase difference between adjacent axial OCT scans (A-scan), PRDOCT greatly improves the detection sensitivity for imaging the flow velocity by decoupling the spatial resolution and velocity sensitivity.

The initial implementation of PRDOCT was based on Hilbert transform, in which the phase of the Doppler signal is determined through the analytic continuation of the measured interference signals by Hilbert transform. By this implementation, a minimum velocity sensitivity as low as $10\,\mu$m/s with a spatial resolution of $10\,\mu$m/s was reported. Moreover, by comparing the sequential A-sans at the same locations, the speckle modulations in the fringe signal cancels each other and will not affect the phase difference calculation.

(c) *Velocity Variance Mode.* One of the main drawbacks of PRDOCT method is that the Doppler shift mainly depends on the angle between the probe beam and flow direction, and which is highly sensitive to the pulsatile nature of the blood flowing through the vessel. In several clinical applications, such as imaging port-wine stain the qualitative flow visualization is more significant than quantitative flow imaging. Zhao et al. extended the use of PRDOCT by introducing the use variance of Doppler frequency spectrum to map the vasculature [112]. One of the main advantages of this velocity variance mapping method is that it eliminates aliasing and can greatly increase the velocity measurement range. Since variance generally increases from the laminar to the turbulent regime, this mode can detect areas of significant turbulence, such as flow near obstructions and bifurcations in vessels; it can also help distinguish true blood flow from bulk tissue motion (e.g., heart wall motion, which typically moves together and thus exhibits low velocity variance). This method gained more attention in different areas of OCT imaging [113, 114]. However, this method cannot provide blood flow directional information. But, by combining this method with the directional information obtained form color Doppler OCT, one can also display directional velocity variance data, similar to the directional power Doppler mode in clinical ultrasound. This method is less sensitive to pulsatile nature of blood flow and provides better visualization of vasculature. The authors demonstrated the feasibility study of this extended technique for the evaluation of the efficiency of PWS in situ laser therapy.

(d) *Histogram-Based Motion-Compensated DOCT.* The sample movement during *in vivo* imaging condition is an inevitable artifact in Doppler-based OCT system and which is particularly very dominant for the case of *in vivo* imaging of human or animals. The relative sample motion represents as a Doppler shift in the light frequency between the light it emits and that it receives. This shift is imparted when the light strikes an object which is moving, relative to the sample probe beam. In case of flow imaging with DOCT, the Doppler frequency due to the involuntary sample motion is depicted as an additional modulation frequency, and this decisive frequency mixing in the interferogram may contribute erroneous result. Yang et al. proposed an approach based on velocity histogram analysis to eliminate this artifact [115]. This approach is based on color Doppler imaging (spectrogram) method, in which the mean Doppler frequency shift along each depth scan is derived using STFT, then the most prominent peak with an arrow velocity distribution is then probably due to bulk tissue motion, and can be eliminated from further analysis. This method is capable of eliminating motion artifacts both faster and slower than the blood flow velocity. More detailed explanation of implementation, performance of this method can be found in the original literature [113, 115].

(e) *Power Doppler OCT (Doppler Amplitude OCT).* Power Doppler OCT (Doppler amplitude OCT) is a functional extension of DOCT which provides an additional contrast mechanism for the visualization of flow based on the concentration of moving scatters as a function of position. This method is widely used in ultrasound imaging field for flow mapping, in which Amplitude is integrated to reflect the power/energy of the autocorrelation signal. Moger et al. first introduced this method [116] and described the data processing steps involved in producing a Doppler amplitude image in OCT. They demonstrated the feasibility of this method for measuring changes in the concentration distribution of red blood cells in glass capillary tubing.

In DAOCT, this source of contrast is sensitive to the density of scatterers rather than their velocity and gives a useful additional parameter for characterizing flow distributions. In order to calculating the Doppler amplitude signal, the digitized interferometric signal is analyzed using STFT. The Doppler amplitude signal can be extracted by calculate the relative area enclosed under the Doppler peak in an STFT. This signal is proportional to the total backscattering coefficient of the medium at a particular velocity (or range of velocities) and can be thought of as OCT but with a spatially varying and adaptive demodulation frequency. Although this method is popular in ultrasound and feasible for microcirculation imaging,this mode turns out to be

rather more computationally intensive in D-OCT because of the complex nature of noise due to bulk tissue motion. It must, therefore, be computed during postprocessing and does not appear well suited for D-OCT real-time imaging.

(2) Frequency Domain-Based DOCT

(a) *Spectral Domain/Swept Source PRDOCT.* Recent development of Fourier domain OCT imaging technique such as spectral domain and swept-source-based imaging technique has made an important step further for PRDOCT from laboratory research into visualization and monitoring of the dynamic blood flow within living tissue *in vivo*. This is largely due to the reason that FDOCT has a significant advantage in detection sensitivity over its time domain counterpart [117–119], leading to increased imaging speed that is essential for any *in vivo* imaging applications. PRDOCT based on time-domain has been successful developments in many *in vivo* imaging applications [106, 111, 120, 121], especially in visualizing microvasculatures within human retina [121, 122].

The spectral domain-based PRDOCT was first proposed by two groups, Leitgeb et al. [103] at Vienna medical university and White et al. [102] at MGH-Harvard. Leitgeb et al. [103] combined the SD-OCT system with a commercial fundus camera-based scanning apparatus to demonstrate the capability of PRDOCT to measure *in vivo* real-time human retinal tissue perfusion with a speed of 25,000 A-scans per second. Using a custom-built SD-OCT imaging system a fast camera, White et al. [102] obtained an A-scan rate of 29,000 per second. The phase-sensitive images were constructed by determining the phase difference between the points at the same depth in adjacent A-scans, which is very similar to the time-domain PRDOCT pioneered by Zhang and chen. Zhang and chen first demonstrated the feasibility of swept-laser-source-based Doppler OCT for *in vivo* imaging of micro circulation [123]. The demonstrated system with swept laser source has a sweep frequency of 2000 A-scans per second. The phase-resolved signal processing method which was implemented previously with their time-domain system was adopted to acquire the velocity and standard deviation images. Doppler and Doppler variance images of fluid flow through glass channels and blood flow through the vessels of a chick chorioallantoic membrane (CAM) were demonstrated *in vivo*. A similar modality called phase-resolved frequency domain imaging was developed by Vakoc et al. [124]. There are other technical developments were reported in the field of frequency domain PRDOCT [125, 126].

Although PRDOCT method could potentially achieve high spatial resolution and high sensitivity for imaging blood flow, its practical *in vivo* imaging performance is however so far being disappointing [127]. The responsible factors that degrade the *in vivo* imaging performance of PRDOCT are that (1) the biological tissue is generally of optical heterogeneous. This sample heterogeneous property imposes a characteristic texture pattern artifact overlaid onto the PRDOCT flow images [128] that masks the slow blood flow signals that would otherwise be detected by the method. (2) *In vivo* sample is always in constant motion, for example, due to heart beat. Thus, the motion artifacts in the PRDOCT blood flow images are inevitable [127].

(b) *Resonant Doppler Flow Imaging.* Resonant Doppler imaging is an alternative approach implemented in Spectral-domain OCT for *in vivo* microcirculation imaging [129]. This method overcomes the fringe blurring artifact which is caused by the sample movement during camera integration and cause drastic reduction of sensitivity for microcirculation measurement. The proposed method was based on introducing a phase shift into the reference arm of the SD-OCT using an electro-optic element to compensate the phase shift introduced by the sample arm movement. By this method, the maximum detectable sensitivity has been shifted effectively to the reference arm velocity, and the maximum detectable velocity is independent of the Nyquist limit given by half the camera acquisition rate. The system can be turned to any particular velocity or associated Doppler frequency for which the sample Doppler frequency will be in resonance. The proposed modality is cable of imaging microcirculation in biological specimens with high contrast where the signals of static structures and sample movements were filtered out. However, this method is insensitive to directional flow and the use of electro-optics modulators makes the system more complex and expensive.

(c) *Joint Spectral and Time Domain OCT (STdOCT).* The Joint Spectral and Time-domain OCT (STdOCT) is another FD-OCT-based flow imaging technique to retrieve microcirculation flow velocity and mapping [130]. In the STdOCT technique, the OCT signal is acquired while the object is scanned laterally with sufficient oversampling for Doppler signal analysis. The oversampling depends upon the ratio between the beam diameter and the scanning step size. By this way, the spectral interference fringes are acquired over time. Then, the two-dimensional Fourier transformation is applied to the spectral OCT signal. The Fourier transform along the wave number axis generates structural images similar to conventional spectral-domain OCT tomograms, and the transformation along the time axis provides information about Doppler beating frequencies corresponding to flow velocities in the object. However, this method requires high sampling density of A-scans along the B-scan direction which requires tremendous amount of time and limits the acquisition frame rate for *in vivo* imaging. But STdOCT technique is more robust for lower SNR, and since it is not phase based, it is less susceptible to motion artifacts.

(d) *Optical Microangiography (OMAG)/Doppler Optical Microangiography (DOMAG).* Optical microangiography (OMAG) [131, 132] is a recently developed imaging method, capable of resolving 3D distribution of dynamic blood perfusion at the capillary level within microcirculatory beds *in vivo*. The imaging contrast of blood perfusion is based on the endogenous light scattering from the moving blood erythrocytes in the blood vessels; thus, no exogenous

contrasting agents are necessary. This is achieved by efficient separation of the moving scattering elements from the static scattering ones within tissue through the OMAG hardware associated with mathematical analysis of the optical scattering signals emerged from an illuminated tissue sample. In the early version on OMAG, the Doppler modulation frequency was introduced by mounting the reference mirror in the reference arm onto a linear Piezo-translation stage [131], which moves the mirror at a constant velocity across the B scan (i.e., x-direction scan). Later, this modulation frequency is introduced by offsetting the sample arm signal light from the x-galvo scanner pivot [133]. However, the latest version of OMAG utilizes the spatial modulation frequency provided by the inherent blood flow modulation rather than reference arm modulation [134, 135]. A detailed overview of this modality can be seen in the literature [136].

In OMAG, the structural and microcirculatory flow images are simultaneously obtained by the spatial filtering of the captured oversampled B-scan interferograms with a modified Hilbert transform algorithm. If we consider an oversampled B-fame, the nonmoving scatters at a depth do not vary with the B-scan time. So, the intensity captured by the CCD camera will be modulated by the heterogeneous properties of the tissue sample along each B-scan. This spatial frequency components of a static tissue sample, that is, the heterogeneous frequencies, will exhibit as a randomly distributed function around zero frequency with a bandwidth of BW. On the other hand, the moving scatters produce a frequency shift, which is caused by the Doppler effect of the moving particles and shifts it away from the heterogeneous frequencies of static scatters. The structural signal is filtered out in the frequency domain. The cut-off frequency depends upon the heterogeneity of the static scatters. Then, the Hilbert transform is used to convert the flow signal to an analytic signal, which includes both amplitude and a phase of the flow signal. For the flow signal, the inverse Fourier transforms have positive and negative frequency. After inverse transforming from frequency domain, by applying the conventional spectral Fourier transform along the depth direction retrieve the strength of the flow signal. Based on the above signal processing, the real flow signal is transformed to an analytic signal by Hilbert transform, which enables the bidirectional flow configuration, that is, the positive flow and the negative flow, can be separated in different imaging plane. OMAG is an emerging imaging modality with clear potential applications in many basic research and medical imaging applications. Because of its exceptionally high spatial resolution and velocity sensitivity, OMAG can provide useful information regarding microcirculation in a number of applications, both in clinical [136, 137] and basic research [138]. Tao et al. implemented a single-pass volumetric bidirectional blood flow imaging- (SPFI-) based spectral domain OCT, the signal processing employed is very analogous the above mentioned method.

One of the key advantages of OMAG is that only the signals backscattered by the functional blood appear in the OMAG flow output plane; this makes the blood flow imaging almost free of artifact-induced noises. However, the early version of OMAG is incapable of providing flow velocity information like Phase Resolved Doppler OCT (PRDOCT). This is because in the OMAG flow image, the regions that are occupied by the microstructural signals are rejected by OMAG; thus, the required correlation between the adjacent A-scans within the static tissue regions is totally lost, leading to a rather noisy appearance in the output plane of flow velocity. To overcome this problem, a digitally reconstruct ideal static background tissue, that is, totally optically homogeneous was replaced with the real heterogeneous tissue sample. This ideal background tissue provides a constant background signal that makes the adjacent A-scans totally correlated, leading to a dramatic increase of the phase signal to noise ratio (SNR) for the phase-resolved signals that represent flow velocities. This method inherits the advantages of both OMAG and PRDOCT. The feasibility of DOMAG for imaging cerebral blood perfusion in mice *in vivo* [134] was demonstrated successfully. Finally, it shows that the *in vivo* performance of DOMAG imaging of blood flow is superior to the traditional PRDOCT. To show the advantages of DOMAG in imaging the blood flow velocities over PRDOCT, a 3D comparison of DOMAG and PRDOCT images were evaluated from a scanned tissue volume from the mouse brain cortex with the skull left intact. Figure 8 shows the OMAG image of cortical brain in mouse with intact skull *in vivo*.

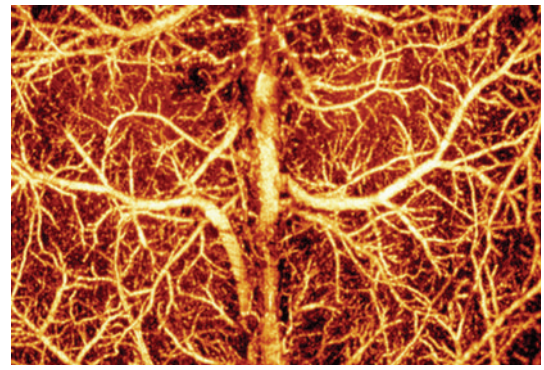

Figure 8: OMAG image of cortical brain in mouse with intact skull *in vivo* (enface view of maximum projection image with volumetric data).

(e) *Digital Frequency Ramping (DFRM).* The Digital frequency ramping method (DFRM) is based on the principle of B-scan phase modulation thresholding, which is initially proposed by Wang by taking the Hilbert transform in the transverse direction of B-frames to obtain bidirectional flow information [139]. Yuan et al. further developed and employed a solely numerical approach-based computer-generated numerical Doppler frequency to enhance flow detection sensitivity and resolution [140]. DFRM is a purely numerical approach for enhanced bidirectional microcirculation imaging, which can be easily implemented on as standard SD-OCT setup to provide 2D and even 3D optical angiography in real-time.

In DFRM method, a phase shift is introduced into the original spectral interferogram using a numerical method based on Hilbert transform. Then, an arbitrary digital Doppler frequency is introduced into the new spectral interferogram signal, which is derived from the Hilbert transform. By this method, a constant Doppler frequency can be introduced into the standard spectral domain interferogram without any hardware implementations such as scanning reference mirror or mirror offsetting at the sample arm. Moreover, DFRM technique enables quantitative flow imaging, which is crucial to a wide variety of physiological and functional imaging studies where quantitative microcirculatory blood flow monitoring is required. Nevertheless, DFR is also subject to limitations because it required computationally intense calculations, which involves multidimensional Hilbert transform and FFT.

3.2. Speckle Variance-Based OCT. The Doppler-based OCT is a powerful tool for quantitative mapping of blood flow in various applications such as skin perfusion imaging, ocular flow imaging, and so forth. However, D-OCT method only determines the axial flow component parallel to the imaging direction of the probe beam. This parallel component of velocity is decided by the relative angle between the flow direction and the imaging beam, which is shown in the Figure 6, and the actual velocity calculation can be obtained by knowing this relative angle. In DOCT, the flow image contrast is mainly determined by this relative angle, and the flow contrast should be maximum when this angle is $\theta \sim 0$, and the contrast vanishes when $\theta \sim 90$. In certain case such as ocular imaging, the primary direction of flow is nearly perpendicular to the imaging beam, which drastically reduces the imaging flow contrast and only vessels with large flow, which have enough axial component to surpass the phase noise can only be imaged. Thus DOCT method is insensitive to provide enough flow contrast to capillaries and small blood vessel with flow direction normal to the imaging beam direction. In order to overcome this limitation, an alternative imaging modality based on time-varying speckle phenomenon was introduced to extract flow information form OCT signal.

The speckle phenomenon is based on the coherence property of the optical waveform which came into prominence with the invention of the laser. Rigorously, a speckle pattern is a random intensity pattern which is produced by the mutual interference of a set of wavefronts. Since the principle of OCT is based on low coherence interferometry, the speckle phenomenon in OCT is inherently relies on the temporal and spatial coherence properties of the optical signal back reflected from the biological tissues. Initially speckle is often regarded as a nuisance, or noise, and it takes several decades for the researchers to realize the full significance of speckle and its applications in various fields. Goodman describes and analyses the statistical properties of laser speckle patterns [141], which is very significant for the conceptualization of speckle contrast imaging, one of the most promising laser-based noninvasive optical image techniques that has been widely used for imaging *in vivo* blood flow dynamics and vascular structure with high spatial and temporal resolution. The potential applications of laser speckle contrast imaging were soon being developed, including the use of time-varying speckle patterns to detect and measure movement. Although the approach of the speckle techniques seems to be completely different from that of Doppler methods, a mathematical analysis shows that the two approaches are, in fact, identical.

3.2.1. Principle of Speckle Contrast Imaging. The speckle contrast imaging modalities in OCT are based on the mathematical analysis of the dynamic speckle pattern generated by the motion of erythrocytes in capillary tissue bed and vessels. Using conventional laser speckle imaging, the flow map of the blood circulation can be obtained either by measuring the spatial contrast [49–51] of the intensity variations or by measuring temporal contrast [52–54] of the intensity variations of the captured images. Each method has its own advantages and disadvantages; the spatial contrast offers superior temporal resolution at the expense of spatial resolution and vice versa for temporal contrast, while the advantages of both can be obtained with spatiotemporal algorithms.

The statistical property of speckle in OCT is very similar the laser speckle imaging [144]. In case of OCT, if we consider the propagation of a focused beam into the capillary bed of the imaging tissue (Figure 9(a)), there are two important cases to be considered for the back scattered sample field signal: (1) the effects of multiple scattering by moving red blood cells within a vessel and (2) the effects of multiple scattering by fixed scatterers located above the flowing red-cell column. Effect (1) will lead to a detected photon experiencing multiple Doppler shifts, producing an apparent flow velocity that is incorrect. Effect (2) will lead to an apparent path length increase for the detected photon and may also distort the angle-of-incidence between the photon and the flow velocity direction, thus leading to an erroneous velocity measurement. Because of the movement of erythrocytes, the multiple scattering causes the fluctuation of speckle pattern spatially and as well as temporally. It is, thus, important to quantify the effects of scattering on D-OCT images.

The spatiotemporal fluctuation caused by the movement of erythrocytes can be directly expressed into the interferogram signal in terms of the optical path difference between the sample and reference arm. Generally, in laser speckle contrast imaging the contrast is defined as the ratio of the standard deviation to the mean intensity

$$K_s = \frac{\sigma_s}{\langle I \rangle}, \tag{9}$$

where K_s is the spatial speckle contract and σ_s refers to the spatial standard deviation of the speckle intensity. Similarly, in case of temporal K_t is the temporal contrast and σ_t refers to the temporal standard deviation. Thus, the flow imaging techniques that are developed for laser speckle contrast imaging can be directly adapted to flow imaging with OCT. However, unlike conventional laser speckle imaging, OCT acquire longitudinal cross-sectional images (B-scan, as

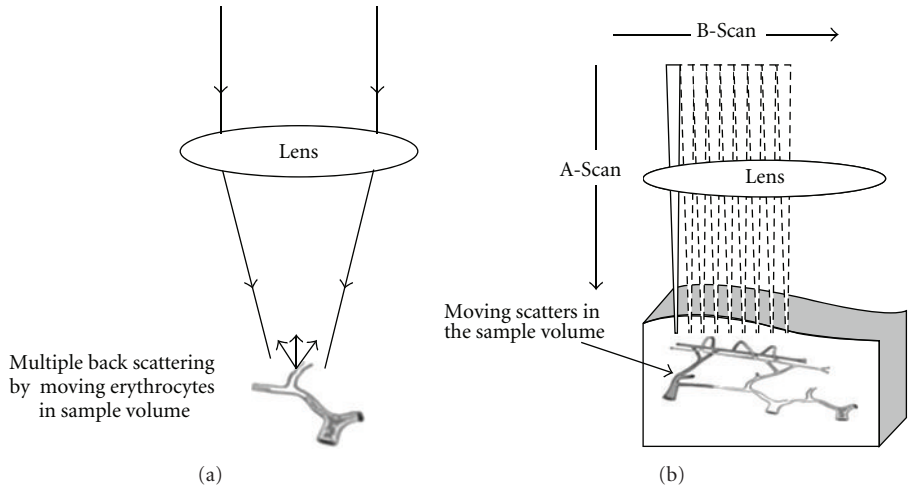

Figure 9: (a) Sample arm beam propagation into the microvascular bed with in the tissue sample. (b) Schematic of a cross-sectional B-scan pattern on the tissue sample.

shown in Figure 9(b)) in a pixel-by-pixel manner; thus, the integration time is relatively longer than camera-based laser speckle imaging. Therefore, in general, the speckle-based OCT flow imaging can be obtained by treating the sequential pixels in the A-scans or B-scan as the sampling of the time varying speckle patterns.

3.2.2. Speckle Contrast-Based OCT Flow Imaging Modalities. Speckle contrast based OCT microvascular imaging is crucial for clinical imaging conditions, where quantitative flow information are not required. The practical implementation of this technique is simpler than conventional DOCT method. Since the image contrast mechanism of speckle OCT is independent of Doppler angle, this method can provide more visually contrast image than D-OCT. In the below section, we will describe various implementation of speckle contrast OCT based on time and frequency domain modalities.

(1) Time Domain Speckle Contrast Imaging Modalities

(a) *Flow Imaging without Phase (Speckle Contrast-Based Imaging).* The peculiarities of the manifestation of the time varying speckle contrast for imaging flow were first introduced by Barton and Stromski in the OCT field [145]. Unlike Doppler-based flowing, this method utilizes the analysis of time varying bio-speckles formed by the moving erythrocytes to quantify the flow information in a depth-resolved manner. This method has the added advantage that it is insensitive to Doppler angle and eliminates the need for phase-sensitive detection to extract the flow information. The first demonstration of this speckle-based flowing was based on a time-domain OCT system. For obtaining the speckle contrast in a B-fame, four captured sequential A-scans in the B-frame were averaged to a single vale to reduce the effect of noise and the single-pixel speckle caused by the wide angle multiple scattering. Then, the signal is converted in to frequency domain to filter out the DC and unwanted frequency components. The filtered signal was then divided evenly into 5 bins with different frequency bands, a low to high frequency ration was calculated to obtain the speckle contrast imaging [146]. However, the initial performance of this method was hindered by the computational complexity of the flow algorithm employed and the relatively slow frame rate of the time-domain OCT system. Another major drawback of the speckle measurement is that it cannot provide the directional flow information like D-OCT.

(2) Frequency Domain Speckle Contrast Imaging

(a) *Microvascular Imaging Based on Motion Contrast Technique.* This method was first introduced by Fingler et al. to demonstrate the ability of a new scanning protocol and phase variance technique to resolve the motion associated with transverse flow [147], which is not easily resolved using conventional Doppler-based OCT technique. This contrast technique is capable of spatially identifying the locations of motion within the imaging specimen associated with vasculature. In their first study, the authors demonstrated two phase variance analysis techniques capable of identifying regions of contrast based on the motion of the scatters without any degradation to the transverse resolution.

Firstly, by capturing multiple M-scans taken over different transverse positions (MB-scan) to create a 2D OCT image, by this scanning modality additional temporal information of the scatter motion could be obtained to improve the motion contrast. However, increasing the amount of A-scans taken within each M-scan not only increases the maximum time between phase images that can be measured, but the improved statistics can increase the dynamic range of standard Doppler flow imaging. This scanning protoaol requires significantly more time per transverse position compared to the original Doppler technique in order to get adequate motion contrast. The increased M-scan time limits the ultimate speed for 2D phase contrast imaging

with this technique, which cannot be improved through improvements to the A-scan acquisition speed. However, quantitative information about the mobility of the scatterers can be determined by the variance of the phase changes for a range of time separations.

Secondly, by acquiring multiple M-scans over different transverse positions to create a 2D OCT image (BM-Scan) and taking the phase differences between successive B-scans, the data throughput of phase contrast images is increased and the phase variance motion contrast can be increased as well. In order to ensure a constant time separation between phase measurements for each transverse location and maintain consistency of contrast across the image, successive B-scans are used for transverse scans of the same direction (every 2nd image from bidirectional scanning or unidirectional scan with flyback). By increasing the time separation between phase measurements such as with sequential B-scans, the sensitivity to slower flows is increased significantly while faster flows maintain high variance contrast which can saturate due to phase wrapping [148]. While quantitative flow information may be lost for scatterers that experience significant phase wrapping for this time separation, the variance contrast ensures the visualization of these regions. In order to reduce the motion noise created by transverse sample motion, a histogram-based noise analysis method was implemented.

(b) *Speckle Variance-Based Microvascular Imaging.* Mariampillai et al. introduced a computationally efficient microvascular imaging based on interframe speckle variance in a swept-source OCT system [142, 149]. Unlike the spatial frequency analysis method reported by Barton et al., this method calculates the interframe intensity variance of structural images, where the image contrast mainly depends on the different time varying properties of fluid versus solid tissue components. The main advantage of this method with respect to DOCT is its signal processing simplicity and implementation. Moreover, this modality is insensitive to Doppler angle-dependent contrast. One of the key disadvantages of this method is the interframe bulk tissue motion, and which can dominate the speckle variance. This motion artifacts could be suppressed by histogram-based method. Figure 10 demonstrates *in vivo* detection of blood flow in vessels as small as 25 μm in diameter using speckle variance method in a dorsal skinfold window chamber model of mice and which is directly compared with intravital fluorescence confocal microscopy.

(c) *Rapid Volumetric Angiography.* This method is very similar to the interframe speckle variance-based microcirculation imaging [137], however, which was implemented in a spectral domain OCT setup. The scanning protocol employed in this technique samples the same transverse location twice per volume with 512 A-scans per image with an interframe sampling time of 11 ms between adjacent B-scans, and thus requires only 12 seconds to render a 3D data set. The angiogram is constructed by high-pass filtering the images along the slow axis of the raster scan [150]. However, this measurement is highly sensitive to the phase shift introduced by the positional errors which includes the sample motion, environmental vibrations, galvanometer jitter, and so forth. The axial movement of the sample causes phase shift and speckle decorrelation in the captured interferograms. These phase variations were estimated and corrected for each transverse position using a cross-correlation method.

(d) *Ultrahigh Sensitive OMAG (OMAG).* The velocity sensitivity of conventional OMAG is determined by the time interval between the adjacent A-scans, and, hence, the high-speed imaging requirement for 3D angiograms limits the sensitivity to slow flow in OMAG. In order to overcome this limitation, a new scheme called UHS-OMAG was intruded. Unlike conventional OMAG, to achieve ultrahigh sensitive imaging of slow microcirculation, UHS-OMAG employs a new scanning protocol and novel flow reconstruction algorithm [143, 151].

UHS-OMAG acquires low density B-scan frame (i.e., x-direction scan) with 128 A-lines with a spacing of ~11.5 μm (which is of the order of the least sampling distance of 10 μm for the system lateral resolution of 16 μm) between adjacent A-lines, which covers a total x-scan range of ~1.5 mm. In this system, the integrating time was set at 17 μs and the maximum line rate of the camera was 47 KHz, which corresponds to a theoretical imaging rate of 367 frames per second (fps). However, by using Camera Link TM and a high-speed frame grabber board (PCI 1428, National Instruments, USA), the maximum achievable frame rate was 300 fps, limited by the hand shake time between the camera and the host computer. A high density C-scan (i.e., in Y-direction), which encompasses 1500 B-scan over a range of 2 mm along the Y-direction with an oversampling factor of ~12. The spacing between adjacent B-scans was ~1.3 μm. The system requires only ~5 seconds to capture a 3D volume data set of a whole imaging sample.

For obtaining slow microcirculation within the capillary vessels, UHS-OMAG algorithm uses high-pass filtering along the C-scan direction similar to the above-discussed method used in the rapid volumetric angiography, rather than in the B-scan direction in conventional OMAG. In UHS-OMAG, thus, the maximum detectable velocity that is not wrapped is determined by the adjacent time spacing between adjacent B-scans in the Y-scan direction. Figure 11 shows the feasibility of UHS-OMAG for *in vivo* imaging of slow microcirculation within the mice cochlea.

4. Summary

The last decade have seen a tremendous development of endogenous-based high resolution and high sensitive optical imaging technique in the field of microcirculation imaging, and numerous studies have shown the feasibility of these modalities in various clinical and fundamental studies. In this paper, we have given an overview of various microcirculation imaging based on endogenous optical imaging techniques. Future improvement of microcirculatory imaging based on laser speckle imaging, capillaroscopy,

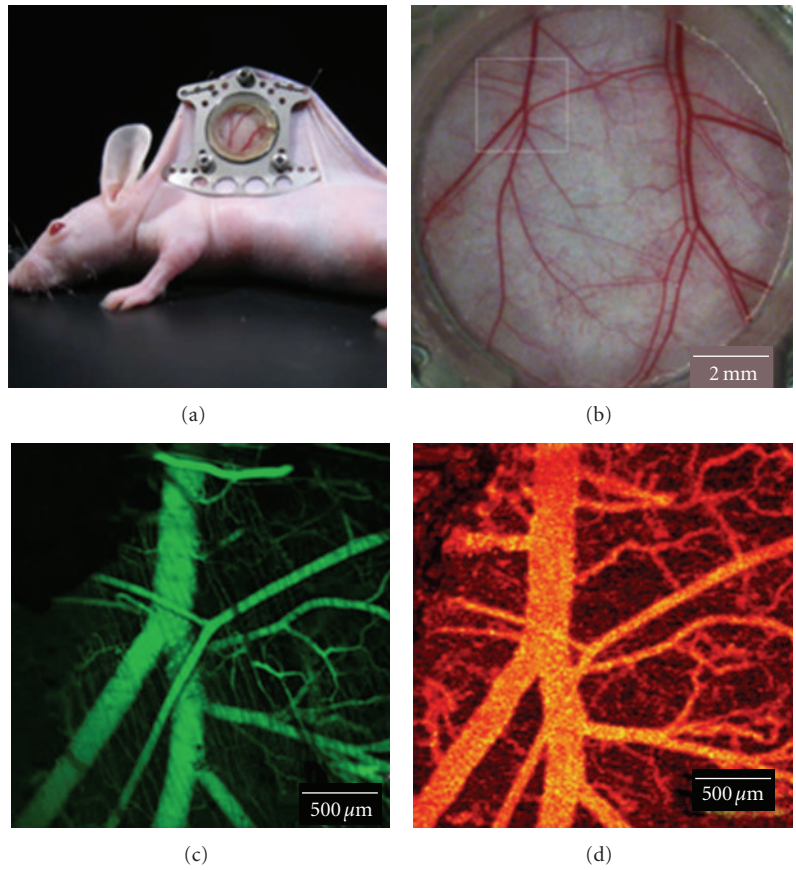

Figure 10: (a) Dorsal skin-fold window chamber model (WCM). (b) White light microscopy of entire window. The white box represents the approximate location of confocal and OCT imaging. (c) Maximum intensity projection image of a fluorescence confocal z stack obtained using 500 kD fluorescein-labeled dextran (1.8×1.8 mm). (d) Speckle variance OCT en face projection image of vasculature without the use of any external contrast agents (1.8×1.8 mm). Image is reproduced from [142]

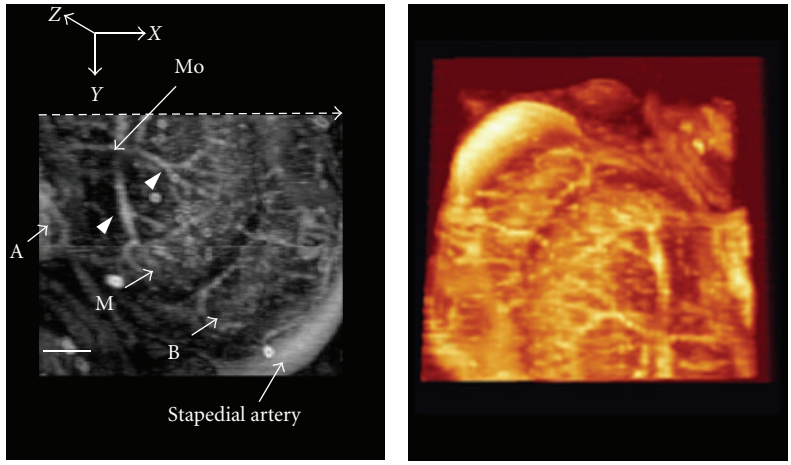

Figure 11: (a) 3D volumetric projection image of the cochlear microvascular network. The vessels imaged here are of the modiolus (Mo) and the otic capsule, lateral wall, and stria vascularis of the cochlear turns that were located within the penetration depth of our imaging system. Apical vessels (A), middle turn vessels (M), and basal turn vessels (B). Radiating arterioles over the middle turn are indicated by *arrowheads*. (b) 3D volumetric perfusion image of the entire cochlea imaged. Image is reproduced from [143].

laser Doppler perfusion imaging, laser speckle perfusion imaging, and polarization spectroscopy will be made by incorporation of more advanced camera technology in terms of resolution and frame rate, which will enable RBC velocity measurements in high flow vessels and more accurate vessel geometry determination with high sensitivity. Moreover, the advancement of completely automated software, with new microcirculatory scoring systems, will lead to faster and more exact determination of microcirculatory functioning in clinical and experimental settings. Emerging noninvasive imaging techniques such as PAT and OCT has potentially broad applications in microvascular imaging and characterization, yet much effort must still be invested to mature this technology.

The development of advanced light sources, beam delivery, new signal processing algorithms, and detection technologies has driven investigations into a wide array of clinical applications of PAT- and OCT-based microvascular imaging techniques in the fields of ophthalmology, cardiology, and oncology, among many others.

References

[1] N. A. Mortillaro and A. E. Taylor, *The Pathophysiology of the Microcirculation*, CRC Press, 1994.

[2] P. G. Camici, "Positron emission tomography and myocardial imaging," *Heart*, vol. 83, no. 4, pp. 475–480, 2000.

[3] P. R. Schvartzman and R. D. White, "Magnetic resonance imaging," in *Textbook of Cardiovascular Medicine*, E. J. Topol, Ed., pp. 213–1256, Lippincott Williams and Wilkins, Philadelphia, Pa, USA, 2nd edition, 2002.

[4] A. B. Hertzman and C. R. Spealman, "Observation on the finger volume pulse recorded photoelectrically," *American Journal of Physiology*, vol. 119, p. 334, 1937.

[5] A. V. J. Challoner, "Photoelectric plethysmography for estimating cutaneous blood flow," in *Non-Invasive Physiological Measurements*, P. Rolfe, Ed., vol. 1, p. 125, Academic Press, London, UK, 1979.

[6] G. Holti and K. W. Mitchell, "Estimation of the nutrient skin blood flow using a non-invasivesegmented thermal probe," in *Non-Invasive Physiological Measurements*, P. Rolfe, Ed., vol. 1, p. 113, Academic Press, London, UK, 1979.

[7] S. S. Kety, "Measurement of regional circulation by the local clearance of radioactive sodium," *American Heart Journal*, vol. 38, no. 3, pp. 321–328, 1949.

[8] P. Sejrsen, "Measurement of cutaneous blood flow by freely diffusible radioactive isotopes. Methodological studies on the washout of krypton-85 and xenon-133 from the cutaneous tissue in man," *Danish Medical Bulletin*, vol. 18, Supplement, pp. 3–38, 1971.

[9] W. Groner, J. W. Winkelman, A. G. Harris et al., "Orthogonal polarization spectral imaging: a new method for study of the microcirculation," *Nature Medicine*, vol. 5, no. 10, pp. 1209–1213, 1999.

[10] R. G. Nadeau and W. Groner, "The role of a new noninvasive imaging technology in the diagnosis of anemia," *Journal of Nutrition*, vol. 131, no. 5, p. 1610S, 2001.

[11] H. Wayland and P. C. Johnson, "Erythrocyte velocity measurement in microvessels by a two-slit photometric method," *Journal of Applied Physiology*, vol. 22, no. 2, pp. 333–337, 1967.

[12] A. Bollinger, P. Butti, and J. P. Barras, "Red blood cell velocity in nailfold capillaries of man measured by a television microscopy technique," *Microvascular Research*, vol. 7, no. 1, pp. 61–72, 1974.

[13] J. G. Stevenson, M. A. Brandestini, T. Weiler, E. A. Howard, and M. Eyer, "Digital multigate Doppler with color echo and Doppler display—diagnosis of atrial and ventricular septal defects," *Circulation*, vol. 60–62, p. 205, 1979.

[14] E. Z. Zhang, J. G. Laufer, R. B. Pedley, and P. C. Beard, "In vivo high-resolution 3D photoacoustic imaging of superficial vascular anatomy," *Physics in Medicine and Biology*, vol. 54, no. 4, pp. 1035–1046, 2009.

[15] V. V. Tuchin, Ed., *Handbook of Optical Biomedical Diagnostics*, vol. PM107, SPIE Press, Bellingham, Wash, USA, 2002.

[16] T. Vo-Dinh, Ed., *Biomedical Photonics Handbook*, CRC Press, Boca Raton, Fla, USA, 2003.

[17] V. V. Tuchin, *Tissue Optics: Light Scattering Methods and Instruments for Medical Diagnosis*, vol. PM 166, SPIE Press, Bellingham, Wash, USA, 2nd edition, 2007.

[18] B. E. Bouma and G. J. Tearney, Eds., *Handbook of Optical Coherence Tomography*, Marcel-Dekker, New York, NY, USA, 2002.

[19] V. V. Tuchin, Ed., *Coherent-Domain Optical Methods for Biomedical Diagnostics, Environmental and Material Science*, vol. 1-2, Kluwer Academic Publishers, Boston, Mass, USA, 2004.

[20] M. Bhushan, T. Moore, A. L. Herrick, and C. E. M. Griffiths, "Nailfold video capillaroscopy in psoriasis," *British Journal of Dermatology*, vol. 142, no. 6, pp. 1171–1176, 2000.

[21] P. Butti, M. Intaglietta, H. Reimann, C. Holliger, A. Bollinger, and M. Anliker, "Capillary red blood cell velocity measurements in human nail fold by video densitometric method," *Microvascular Research*, vol. 10, pp. 220–227, 1975.

[22] T. J. Ryan, "Measurement of blood flow and other properties of the vessels of the skin," in *The Physiology and Pathophysiology of the Skin*, A. Jarrett, Ed., vol. 1, pp. 653–679, Academic Press, London, UK, 1973.

[23] B. Fagrell, A. Fronek, and M. Intaglietta, "A microscope-television system for studying flow velocity in human skin capillaries," *American Journal of Physiology*, vol. 233, no. 2, pp. H318–H321, 1977.

[24] P. Dolezalova, S. P. Young, P. A. Bacon, and T. R. Southwood, "Nailfold capillary microscopy in healthy children and in childhood rheumatic diseases: a prospective single blind observational study," *Annals of the Rheumatic Diseases*, vol. 62, no. 5, pp. 444–449, 2003.

[25] T. Ohtsuka, T. Tamura, A. Yamakage, and S. Yamazaki, "The predictive value of quantitative nailfold capillary microscopy in patients with undifferentiated connective tissue disease," *British Journal of Dermatology*, vol. 139, no. 4, pp. 622–629, 1998.

[26] K. A. Kwiterovich, M. G. Maguire, R. P. Murphy et al., "Frequency of adversesystemic reactions after fluorescein angiography. Results of a prospectivestudy," *Ophthalmology*, vol. 98, pp. 1139–1142, 1991.

[27] M. Hope-Ross, L. A. Yannuzzi, E. S. Gragoudas et al., "Adverse reactions due to indocyanine green," *Ophthalmology*, vol. 101, no. 3, pp. 529–533, 1994.

[28] D. De Backer and M. J. Dubois, "Assessment of the microcirculatory flow in patients in the intensive care unit," *Current Opinion in Critical Care*, vol. 7, no. 3, pp. 200–203, 2001.

[29] J. R. Weinberg, P. Boyle, K. Thomas, K. Murphy, J. E. Tooke, and A. Guz, "Capillary blood cell velocity is reduced in fever

without hypotension," *International Journal of Microcirculation, Clinical and Experimental*, vol. 10, no. 1, pp. 13–19, 1991.

[30] B. Fagrell and M. Intaglietta, "Microcirculation: its significance in clinical and molecular medicine," *Journal of Internal Medicine*, vol. 241, no. 5, pp. 349–362, 1997.

[31] B. Fagrell, "Microcirculatory methods for the clinical assessment of hypertension, hypotension, and ischemia," *Annals of Biomedical Engineering*, vol. 14, no. 2, pp. 163–173, 1986.

[32] Z. Chen, Y. Zhao, S. M. Srinivas, J. S. Nelson, N. Prakash, and R. D. Frostig, "Optical Doppler tomography," *IEEE Journal on Selected Topics in Quantum Electronics*, vol. 5, no. 4, pp. 1134–1142, 1999.

[33] M. L. Iabichella, E. Melillo, and G. Mosti, "A review of microvascular measurements in wound healing," *International Journal of Lower Extremity Wounds*, vol. 5, no. 3, pp. 181–199, 2006.

[34] P. H. Carpentier, "Current techniques for the clinical evaluation of the microcirculation," *Journal des Maladies Vasculaires*, vol. 26, no. 2, pp. 142–147, 2001.

[35] J. Lee, A. C. Jirapatnakul, A. P. Reeves, W. E. Crowe, and I. H. Sarelius, "Vessel diameter measurement from intravital microscopy," *Annals of Biomedical Engineering*, vol. 37, no. 5, pp. 913–926, 2009.

[36] W. Groner, J. W. Winkelman, A. G. Harris et al., "Orthogonal polarization spectral imaging: a new method for study of the microcirculation," *Nature Medicine*, vol. 5, no. 10, pp. 1209–1213, 1999.

[37] J. Lndert, J. Werner, M. Redlin, H. Kippe, H. Habazettl, and A. R. Pries, "OPS imaging of human circulation: ashort technical report," *Journal of Vascular Research*, vol. 39, pp. 368–372, 2002.

[38] A. Bauer, S. Kofler, M. Thiel, S. Eifert, and F. Christ, "Monitoring of the sublingual microcirculation in cardiac surgery using orthogonal polarization spectral imaging: preliminary results," *Anesthesiology*, vol. 107, no. 6, pp. 939–945, 2007.

[39] G. Belcaro, U. Hoffmann, A. Bollinger, and A. Nicolaides, *Laser Doppler*, Med-Orion Publishing Company, London, UK, 2003.

[40] M. J. Leahy, F. F. M. De Mul, G. E. Nilsson, and R. Maniewski, "Principles and practice of the laser-Doppler perfusion technique," *Technology and Health Care*, vol. 7, no. 2-3, pp. 143–162, 1999.

[41] C. Riva, B. Ross, and G. B. Benedek, "Laser Doppler measurements of blood flow in capillary tubes and retinal arteries," *Investigative Ophthalmology*, vol. 11, no. 11, pp. 936–944, 1972.

[42] A. Fullerton, M. Stücker, K. P. Wilhelm et al., "Guidelines for visualization of cutaneous blood flow by laser Doppler perfusion imaging," *Contact Dermatitis*, vol. 46, no. 3, pp. 129–140, 2002.

[43] A. Serov, W. Steenbergen, and F. De Mul, "Laser Doppler perfusion imaging with a complimentary metal oxide semiconductor image sensor," *Optics Letters*, vol. 27, no. 5, pp. 300–302, 2002.

[44] A. Serov, B. Steinacher, and T. Lasser, "Full-field laser Doppler perfusion imaging and monitoring with an intelligent CMOS camera," *Optics Express*, vol. 13, no. 10, pp. 3681–3689, 2005.

[45] A. Serov and T. Lasser, "High-speed laser Doppler perfusion imaging using an integrating CMOS image sensor," *Optics Express*, vol. 13, no. 17, pp. 6416–6428, 2005.

[46] M. J. Joyner, N. M. Dietz, and J. T. Shepherd, "From Belfast to Mayo and beyond: the use and future of plethysmography to study blood flow in human limbs," *Journal of Applied Physiology*, vol. 91, no. 6, pp. 2431–2441, 2001.

[47] J. D. Briers, "Laser Doppler, speckle and related techniques for blood perfusion mapping and imaging," *Physiological Measurement*, vol. 22, no. 4, pp. R35–R66, 2001.

[48] A. F. Fercher and J. D. Briers, "Flow visualization by means of single-exposure speckle photography," *Optics Communications*, vol. 37, no. 5, pp. 326–330, 1981.

[49] J. D. Briers and S. Webster, "Quasi real-time digital version of single-exposure speckle photography for full-field monitoring of velocity or flow fields," *Optics Communications*, vol. 116, no. 1-3, pp. 36–42, 1995.

[50] J. D. Briers and S. Webster, "Laser speckle contrast analysis (LASCA): a nonscanning, full-field technique for monitoring capillary blood flow," *Journal of Biomedical Optics*, vol. 1, no. 2, pp. 174–179, 1996.

[51] J. D. Briers, "Time-varying laser speckle for measuring motion and flow," in *Coherent Optics of Ordered and Random Media*, D. A. Zimnyakov, Ed., vol. 4242, pp. 25–39, 2001.

[52] H. Cheng, Q. Luo, S. Zeng, S. Chen, J. Cen, and H. Gong, "Modified laser speckle imaging method with improved spatial resolution," *Journal of Biomedical Optics*, vol. 8, no. 3, pp. 559–564, 2003.

[53] B. Choi, J. C. Ramirez-San-Juan, J. Lotfi, and J. S. Nelson, "Linear response range characterization and *in vivo* application of laser speckle imaging of blood flow dynamics," *Journal of Biomedical Optics*, vol. 11, no. 4, Article ID 041129, 2006.

[54] R. Nothdurft and G. Yao, "Imaging obscured subsurface inhomogeneity using laser speckle," *Optics Express*, vol. 13, no. 25, pp. 10034–10039, 2005.

[55] X. Wang, Y. Xu, M. Xu, S. Yokoo, E. S. Fry, and L. V. Wang, "Photoacoustic tomography of biological tissues with high cross-section resolution: reconstruction and experiment," *Medical Physics*, vol. 29, no. 12, pp. 2799–2805, 2002.

[56] X. Wang, D. L. Chamberland, and D. A. Jamadar, "Noninvasive photoacoustic tomography of human peripheral joints toward diagnosis of inflammatory arthritis," *Optics Letters*, vol. 32, no. 20, pp. 3002–3004, 2007.

[57] X. Wang, Y. Pang, G. Ku, G. Stoica, and L. V. Wang, "Three-dimensional laser-induced photoacoustic tomography of mouse brain with the skin and skull intact," *Optics Letters*, vol. 28, no. 19, pp. 1739–1741, 2003.

[58] K. Maslov, G. Stoica, and L. V. Wang, "*In vivo* dark-field reflection-mode photoacoustic microscopy," *Optics Letters*, vol. 30, no. 6, pp. 625–627, 2005.

[59] S. Hu, K. Maslov, and L. V. Wang, "Noninvasive label-free imaging of microhemodynamics by optical-resolution photoacoustic microscopy," *Optics Express*, vol. 17, no. 9, pp. 7688–7693, 2009.

[60] D. Yang, D. Xing, Y. Tan, H. Gu, and S. Yang, "Integrative prototype B-scan photoacoustic tomography system based on a novel hybridized scanning head," *Applied Physics Letters*, vol. 88, no. 17, Article ID 174101, 2006.

[61] P. Burgholzer, G. J. Matt, M. Haltmeier, and G. Paltauf, "Exact and approximative imaging methods for photoacoustic tomography using an arbitrary detection surface," *Physical Review E*, vol. 75, no. 4, Article ID 046706, 2007.

[62] D. Huang, E. A. Swanson, C. P. Lin et al., "Optical coherence tomography," *Science*, vol. 254, no. 5035, pp. 1178–1181, 1991.

[63] A. F. Fercher, W. Drexler, C. K. Hitzenberger, and T. Lasser, "Optical coherence tomography-Principles and applications," *Reports on Progress in Physics*, vol. 66, no. 2, pp. 239–303, 2003.

[64] W. Drexler and J. G. Fujimoto, Eds., *Optical Coherence Tomography: Technology and Applications*, Springer, Berlin, Germany, 2008.

[65] N. Tanno, T. Ichikawa, and A. Saeki, "Lightwave reflection measurement," Japanese Patent no. 2010042, 1990.

[66] S. Chiba and N. Tanno, "Backscattering optical heterodyne tomography," prepared for the 14th Laser Sensing Symposium, 1991.

[67] J. G. Fujimoto, S. De Silvestri, E. P. Ippen et al., "Femtosecond optical ranging in biological systems," *Optics Letters*, vol. 11, pp. 150–152, 1986.

[68] B. L. Danielson and C. D. Whittenberg, "Guided-wave reflectometry with micrometer resolution," *Applied Optics*, vol. 26, pp. 2836–2842, 1987.

[69] K. Takada, I. Yokohama, K. Chida, and J. Noda, "New measurement system for fault location in optical waveguide devices based on an interferometric technique," *Applied Optics*, vol. 26, pp. 1603–1606, 1987.

[70] A. F. Fercher, K. Mengedoht, and W. Werner, "Eye-length measurement by interferometry with partially coherent light," *Optics Letters*, vol. 13, pp. 1867–1869, 1988.

[71] C. K. Hitzenberger, W. Drexler, and A. F. Fercher, "Measurement of corneal thickness by laser Doppler interferometry," *Investigative Ophthalmology and Visual Science*, vol. 33, no. 1, pp. 98–103, 1992.

[72] J. A. Izatt, M. R. Hee, E. A. Swanson et al., "Micrometer-scale resolution imaging of the anterior eye in vivo with optical coherence tomography," *Archives of Ophthalmology*, vol. 112, no. 12, pp. 1584–1589, 1994.

[73] T. Sawatari, "Optical heterodyne scanning microscope," *Applied Optics*, vol. 12, no. 11, pp. 2768–2772, 1973.

[74] J. M. Schmitt, A. Knüttel, and R. F. Bonner, "Measurement of optical properties of biological tissues by low-coherence reflectometry," *Applied Optics*, vol. 32, no. 30, pp. 6032–6042, 1993.

[75] X. Clivaz, F. Marquis-Weible, R. P. Salathé, R. P. Novak, and H. H. Gilgen, "High resolutionrelfectometry in biological tissues," *Optics Letters*, vol. 17, pp. 4–6, 1992.

[76] G. Häusler and M. W. Lindner, ""Coherence radar" and "spectral radar"—new tools for dermatological diagnosis," *Journal of Biomedical Optics*, vol. 3, no. 1, pp. 21–31, 1998.

[77] E. A. Swanson, J. A. Izatt, M. R. Hee et al., "In vivo retinal imaging by optical coherence tomography," *Optics Letters*, vol. 18, no. 21, pp. 1864–1869, 1993.

[78] M. R. Hee, D. Huang, E. A. Swanson, and J. G. Fujimoto, "Polarization sensitive low-coherence reflectometer for birefringence characterization and ranging," *Journal of the Optical Society of America B*, vol. 9, pp. 903–908, 1992.

[79] E. Götzinger, M. Pircher, and C. K. Hitzenberger, "High speed spectral domain polarization sensitive optical coherence tomography of the human retina," *Optics Express*, vol. 13, no. 25, pp. 10217–10229, 2005.

[80] Y. Yasuno, S. Makita, Y. Sutoh, M. Itoh, and T. Yatagai, "Birefringence imaging of human skin by polarization-sensitive spectral interferometric optical coherence tomography," *Optics Letters*, vol. 27, no. 20, pp. 1803–1805, 2002.

[81] B. H. Park, M. C. Pierce, B. Cense et al., "Real-time fiber-based multi-functional spectral-domain optical coherence tomography at 1.3 μm," *Optics Express*, vol. 13, no. 11, pp. 3931–3944, 2005.

[82] S. Makita, Y. Yasuno, T. Endo, M. Itoh, and T. Yatagai, "Polarization contrast imaging of biological tissues by polarization-sensitive Fourier-domain optical coherence tomography," *Applied Optics*, vol. 45, no. 6, pp. 1142–1147, 2006.

[83] M. Yamanari, S. Makita, V. D. Madjarova, T. Yatagai, and Y. Yasuno, "Fiber-based polarization-sensitive Fourier domain optical coherence tomography using B-scan-oriented polarization modulation method," *Optics Express*, vol. 14, no. 14, pp. 6502–6515, 2006.

[84] M. Yamanari, S. Makita, and Y. Yasuno, "Polarization-sensitive swept-source optical coherence tomography with continuous source polarization modulation," *Optics Express*, vol. 16, no. 8, pp. 5892–5906, 2008.

[85] J. F. De Boer, S. M. Srinivas, A. Malekafzali, Z. Chen, and J. S. Nelson, "Imaging thermally damaged tissue by polarization sensitive optical coherence tomography," *Optics Express*, vol. 3, no. 6, pp. 212–218, 1998.

[86] C. E. Saxer, J. F. De Boer, B. H. Park, Y. Zhao, Z. Chen, and J. S. Nelson, "High-speed fiber-based polarization-sensitive optical coherence tomography of *in vivo* human skin," *Optics Letters*, vol. 25, no. 18, pp. 1355–1357, 2000.

[87] S. Jiao and L. V. Wang, "Two-dimensional depth-resolved Mueller matrix of biological tissue measured with double-beam polarization-sensitive optical coherence tomography," *Optics Letters*, vol. 27, no. 2, pp. 101–103, 2002.

[88] J. Shuliang, Y. Gang, and L. V. Wang, "Depth-resolved two-dimensional Stokes vectors of backscattered light and Mueller matrices of biological tissue measured with optical coherence tomography," *Applied Optics*, vol. 39, no. 34, pp. 6318–6324, 2000.

[89] J. F. De Boer, T. E. Milner, M. J. C. Van Gemert, and J. S. Nelson, "Two-dimensional birefringence imaging in biological tissue by polarization-sensitive optical coherence tomography," *Optics Letters*, vol. 22, no. 12, pp. 934–936, 1997.

[90] Z. Chen, T. E. Milner, D. Dave, and J. S. Nelson, "Optical Doppler tomographic imaging of fluid flow velocity in highly scattering media," *Optics Letters*, vol. 22, no. 1, pp. 64–66, 1997.

[91] Z. Chen, T. E. Milner, S. Srinivas et al., "Noninvasive imaging of *in vivo* blood flow velocity using optical Doppler tomography," *Optics Letters*, vol. 22, no. 14, pp. 1119–1121, 1997.

[92] J. A. Izatt, M. D. Kulkarni, S. Yazdanfar, J. K. Barton, and A. J. Welch, "*In vivo* bidirectional color Doppler flow imaging of picoliter blood volumes using optical coherence tomography," *Optics Letters*, vol. 22, no. 18, pp. 1439–1441, 1997.

[93] S. Yazdanfar, M. D. Kulkarni, and J. A. Izatt, "High resolution imaging of in vivo cardiac dynamics using color Doppler optical coherence tomography," *Optics Express*, vol. 1, no. 13, pp. 424–431, 1997.

[94] M. D. Kulkarni, T. G. Van Leeuwen, S. Yazdanfar, and J. A. Izatt, "Velocity-estimation accuracy and frame-rate limitations in color Doppler optical coherence tomography," *Optics Letters*, vol. 23, no. 13, pp. 1057–1059, 1998.

[95] Z. Ding, Y. Zhao, H. Ren, J. S. Nelson, and Z. Chen, "Real-time phase-resolved optical coherence tomography and optical Doppler tomography," *Optics Express*, vol. 10, no. 5, pp. 236–245, 2002.

[96] S. J. Matcher, M. Cope, and D. T. Delpy, "*In vivo* measurements of the wavelength dependence of tissue-scattering

coefficients between 760 and 900 nm measured with time-resolved spectroscopy," *Applied Optics*, vol. 36, no. 1, pp. 386–396, 1997.

[97] U. Morgner, W. Drexler, F. X. Kärtner et al., "Spectroscopic optical coherence tomography," *Optics Letters*, vol. 25, no. 2, pp. 111–113, 2000.

[98] R. Leitgeb, M. Wojtkowski, A. Kowalczyk, C. K. Hitzenberger, M. Sticker, and A. F. Fercher, "Spectral measurement of absorption by spectroscopic frequency-domain optical coherence tomography," *Optics Letters*, vol. 25, no. 11, pp. 820–822, 2000.

[99] R. Leitgeb, M. Wojtkowski, C. Hitzenberger, A. Fercher, and H. Sattmann, "Spectroscopic analysis of substances by frequency domain optical coherence tomography," in *Coherence Domain Optical Methods in Biomedical Science and Clinical Applications*, vol. 4251 of *Proceedings of SPIE*, pp. 123–127, 2001.

[100] J. Su, I. V. Tomov, YI. Jiang, and Z. Chen, "High-resolution frequency-domain second-harmonic optical coherence tomography," *Applied Optics*, vol. 46, no. 10, pp. 1770–1775, 2007.

[101] M. V. Sarunic, B. E. Applegate, and J. A. Izatt, "Spectral domain second-harmonic optical coherence tomography," *Optics Letters*, vol. 30, no. 18, pp. 2391–2393, 2005.

[102] B. R. White, M. C. Pierce, N. Nassif et al., "*In vivo* dynamic human retinal blood flow imaging using ultra-high-speed spectral domain optical doppler tomography," *Optics Express*, vol. 11, no. 25, pp. 3490–3497, 2003.

[103] R. A. Leitgeb, L. Schmetterer, W. Drexler, A. F. Fercher, R. J. Zawadzki, and T. Bajraszewski, "Real-time assessment of retinal blood flow with ultrafast acquisition by color Doppler Fourier domain optical coherence tomography," *Optics Express*, vol. 11, no. 23, pp. 3116–3121, 2003.

[104] R. A. Leitgeb, L. Schmetterer, C. K. Hitzenberger et al., "Real-time measurement of in vitro flow by Fourier-domain color Doppler optical coherence tomography," *Optics Letters*, vol. 29, no. 2, pp. 171–173, 2004.

[105] S. Makita, Y. Hong, M. Yamanari, T. Yatagai, and Y. Yasuno, "Optical coherence angiography," *Optics Express*, vol. 14, no. 17, pp. 7821–7840, 2006.

[106] Y. Zhao, Z. Chen, C. Saxer, S. Xiang, J. F. De Boer, and J. S. Nelson, "Phase-resolved optical coherence tomography and optical Doppler tomography for imaging blood flow in human skin with fast scanning speed and high velocity sensitivity," *Optics Letters*, vol. 25, no. 2, pp. 114–116, 2000.

[107] R. K. Wang, "High-resolution visualization of fluid dynamics with Doppler optical coherence tomography," *Measurement Science and Technology*, vol. 15, no. 4, pp. 725–733, 2004.

[108] V. Gusmeroli and M. Martinelli, "Distributed laser Doppler velocimeter," *Optics Letters*, vol. 16, pp. 1358–1360, 1991.

[109] F. Hlawatsch and G. F. Boudreaux-Bartels, "Linear and quadratic time-frequency signal representations," *IEEE Signal Processing Magazine*, vol. 9, no. 2, pp. 21–67, 1992.

[110] Z. Chen, T. E. Milner, S. Srinivas et al., "Noninvasive imaging of in vivo blood flow velocity using optical Doppler tomography," *Optics Letters*, vol. 22, no. 14, pp. 1119–1121, 1997.

[111] Y. Zhao, Z. Chen, C. Saxer, S. Xiang, J. F. De Boer, and J. S. Nelson, "Phase-resolved optical coherence tomography and optical Doppler tomography for imaging blood flow in human skin with fast scanning speed and high velocity sensitivity," *Optics Letters*, vol. 25, no. 2, pp. 1358–1360, 2000.

[112] Y. Zhao, Z. Chen, C. Saxer et al., "Doppler standard deviation imaging for clinical monitoring of in vivo human skin blood flow," *Optics Letters*, vol. 25, no. 18, pp. 1358–1360, 2000.

[113] V. X. D. Yang, M. L. Gordon, and B. Qi, "High speed, wide velocity dynamic range Doppler optical coherence omography—part I: system design, signal processing, and performance characterization," *Optics Express*, vol. 11, pp. 794–809, 2003.

[114] V. X. D. Yang, M. L. Gordon, E. Seng-Yue et al., "High speed, wide velocity dynamic range doppler optical coherence tomography (Part II): imaging in vivo cardiac dynamics of Xenopus laevis," *Optics Express*, vol. 11, no. 14, pp. 1650–1658, 2003.

[115] V. X. D. Yang, M. L. Gordon, S. J. Tang et al., "High speed, wide velocity dynamic range doppler optical coherence tomography (part III): in vivo endoscopic imaging of blood flow in the rat and human gastrointestinal tracts," *Optics Express*, vol. 11, no. 19, pp. 2416–2424, 2003.

[116] J. Moger, S. J. Matcher, C. P. Winlove, and A. Shore, "Measuring red blood cell flow dynamics in a glass capillary using Doppler optical coherence tomography and Doppler amplitude optical coherence tomography," *Journal of Biomedical Optics*, vol. 9, no. 5, pp. 982–994, 2004.

[117] M. A. Choma, M. V. Sarunic, C. Yang, and J. A. Izatt, "Sensitivity advantage of swept source and Fourier domain optical coherence tomography," *Optics Express*, vol. 11, no. 18, pp. 2183–2189, 2003.

[118] J. F. De Boer, B. Cense, B. H. Park, M. C. Pierce, G. J. Tearney, and B. E. Bouma, "Improved signal-to-noise ratio in spectral-domain compared with time-domain optical coherence tomography," *Optics Letters*, vol. 28, no. 21, pp. 2067–2069, 2003.

[119] R. Leitgeb, C. K. Hitzenberger, and A. F. Fercher, "Performance of fourier domain vs. time domain optical coherence tomography," *Optics Express*, vol. 11, no. 8, pp. 889–894, 2003.

[120] J. K. Barton, J. A. Izatt, M. D. Kulkarni, S. Yazdanfar, and A. J. Welch, "Three-dimensional reconstruction of blood vessels from *in vivo* color Doppler optical coherence tomography images," *Dermatology*, vol. 198, no. 4, pp. 355–361, 1999.

[121] S. Yazdanfar, A. M. Rollins, and J. A. Izatt, "*In vivo* imaging of human retinal flow dynamics by color Doppler optical coherence tomography," *Archives of Ophthalmology*, vol. 121, no. 2, pp. 235–239, 2003.

[122] S. Yazdanfar, A. M. Rollins, and J. A. Izatt, "Imaging and velocimetry of the human retinal circulation with color Doppler optical coherence tomography," *Optics Letters*, vol. 25, no. 19, pp. 1448–1450, 2000.

[123] J. Zhang and Z. Chen, "In vivo blood flow imaging by a swept laser source based Fourier domain optical Doppler tomography," *Optics Express*, vol. 13, no. 19, pp. 7449–7457, 2005.

[124] B. J. Vakoc, S. H. Yun, J. F. De Boer, G. J. Tearney, and B. E. Bouma, "Phase-resolved optical frequency domain imaging," *Optics Express*, vol. 13, no. 14, pp. 5483–5493, 2005.

[125] L. Wang, Y. Wang, S. Guo et al., "Frequency domain phase-resolved optical Doppler and Doppler variance tomography," *Optics Communications*, vol. 242, no. 4–6, pp. 345–350, 2004.

[126] S. Yazdanfar, C. Yang, M. V. Sarunic, and J. A. Izatt, "Frequency estimation precision in Doppler optical coherence tomography using the Cramer-Rao lower bound," *Optics Express*, vol. 13, no. 2, pp. 410–416, 2005.

[127] S. H. Yun, G. J. Tearney, J. F. De Boer, and B. E. Bouma, "Motion artifacts in optical coherence tomography with frequency-domain ranging," *Optics Express*, vol. 12, no. 13, pp. 2977–2998, 2004.

[128] R. K. Wang and Z. Ma, "Real-time flow imaging by removing texture pattern artifacts in spectral-domain optical Doppler tomography," *Optics Letters*, vol. 31, no. 20, pp. 3001–3003, 2006.

[129] A. H. Bachmann, M. L. Villiger, C. Blatter, T. Lasser, and R. A. Leitgeb, "Resonant doppler flow imaging and optical vivisection of retinal blood vessels," *Optics Express*, vol. 15, no. 2, pp. 408–422, 2007.

[130] M. Szkulmowski, A. Szkulmowska, T. Bajraszewski, A. Kowalczyk, and M. Wojtkowski, "Flow velocity estimation using joint spectral and time domain optical coherence tomography," *Optics Express*, vol. 16, no. 9, pp. 6008–6025, 2008.

[131] R. K. Wang, S. L. Jacques, Z. Ma, S. Hurst, S. R. Hanson, and A. Gruber, "Three dimensional optical angiography," *Optics Express*, vol. 15, no. 7, pp. 4083–4097, 2007.

[132] R. K. Wang and S. Hurst, "Mapping of cerebro-vascular blood perfusion in mice with skin and skull intact by Optical Micro-AngioGraphy at 1.3 μm wavelength," *Optics Express*, vol. 15, no. 18, pp. 11402–11412, 2007.

[133] L. An and R. K. Wang, "*In vivo* volumetric imaging of vascular perfusion within human retina and choroids with optical micro-angiography," *Optics Express*, vol. 16, no. 15, pp. 11438–11452, 2008.

[134] R. K. Wang and L. An, "Doppler optical micro-angiography for volumetric imaging of vascular perfusion in vivo," *Optics Express*, vol. 17, no. 11, pp. 8926–8940, 2009.

[135] L. An, H. M. Subhash, D. J. Wilson, and R. K. Wang, "High resolution wide-field imaging of retinal and choroidal blood perfusion with optical micro-angiography," *Journal of Biomedical Optics*, vol. 15, no. 2, 2010.

[136] R. K. Wang and H. M. Subhash, "Optical microangiography: high-resolution 3-D imaging of blood flow," *Optics and Photonics News*, vol. 20, no. 11, pp. 40–46, 2009.

[137] R. K. Wang, L. An, S. Saunders, and D. J. Wilson, "Optical microangiography provides depth-resolved images of directional ocular blood perfusion in posterior eye segment," *Journal of Biomedical Optics*, vol. 15, no. 2, 2010.

[138] Y. Jia and R. K. Wang, "Optical micro-angiography images structural and functional cerebral blood perfusion in mice with cranium left intact," *Journal of Biophotonics*, vol. 4, no. 1-2, pp. 57–63, 2011.

[139] R. K. Wang, "Directional blood flow imaging in volumetric optical microangiography achieved by digital frequency modulation," *Optics Letters*, vol. 33, no. 16, pp. 1878–1880, 2008.

[140] Z. Yuan, Z. C. Luo, H. G. Ren, C. W. Du, and Y. Pan, "A digital frequency ramping method for enhancing Doppler flow imaging in Fourier-domain optical coherence tomography," *Optics Express*, vol. 17, no. 5, pp. 3951–3963, 2009.

[141] J. W. Goodman, "Statistical properties of laser speckle patterns," in *Laser Speckle and Related Phenomena*, J. C. Dainty, Ed., vol. 9 of *Topics in Applied Physics*, Springer, New York, NY, USA, 1984.

[142] A. Mariampillai, B. A. Standish, E. H. Moriyama et al., "Speckle variance detection of microvasculature using swept-source optical coherence tomography," *Optics Letters*, vol. 33, no. 13, pp. 1530–1532, 2008.

[143] H. M. Subhash, V. Davila, H. Sun et al., "Volumetric *in vivo* imaging of microvascular perfusion within the intact cochlea in mice using ultra-high sensitive optical microangiography," *IEEE Transactions on Medical Imaging*, vol. 30, no. 2, pp. 224–230, 2011.

[144] J. M. Schmitt, S. H. Xiang, and K. M. Yung, "Speckle in optical coherence tomography," *Journal of Biomedical Optics*, vol. 4, no. 1, pp. 95–105, 1999.

[145] J. K. Barton and S. Stromski, "Flow measurement without phase information in optical coherence tomography images," *Optics Express*, vol. 13, no. 14, pp. 5234–5239, 2005.

[146] H. Fujii, T. Asakura, and K. Nohira, "Blood flow observed by time-varying laser speckle," *Optics Letters*, vol. 10, no. 3, pp. 104–106, 1985.

[147] J. Fingier, D. Schwartz, C. Yang, and S. E. Fraser, "Mobility and transverse flow visualization using phase variance contrast with spectral domain optical coherence tomography," *Optics Express*, vol. 15, no. 20, pp. 12636–12653, 2007.

[148] J. Fingler, R. J. Zawadzki, J. S. Werner, D. Schwartz, and S. E. Fraserl, "Volumetric microvascular imaging of human retina using optical coherence tomography with a novel motion contrast technique," *Optics Express*, vol. 17, no. 24, pp. 22190–22200, 2009.

[149] A. Mariampillai, M. K. K. Leung, M. Jarvi et al., "Optimized speckle variance OCT imaging of microvasculature," *Optics Letters*, vol. 35, no. 8, pp. 1257–1259, 2010.

[150] V. J. Srinivasan, J. Y. Jiang, M. A. Yaseen et al., "Rapid volumetric angiography of cortical microvasculature with optical coherence tomography," *Optics Letters*, vol. 35, no. 1, pp. 43–45, 2010.

[151] L. An, J. Qin, and R. K. Wang, "Ultrahigh sensitive optical microangiography for in vivo imaging of microcirculations within human skin tissue beds," *Optics Express*, vol. 18, no. 8, pp. 8220–8228, 2010.